

TRANSPARENT THIN FILM HEATERS
BASED ON SILVER NANOWIRE NETWORKS

A THESIS SUBMITTED TO
THE GRADUATE SCHOOL OF NATURAL AND APPLIED SCIENCES
OF
MIDDLE EAST TECHNICAL UNIVERSITY

BY

ORÇUN ERGÜN

IN PARTIAL FULFILLMENT OF THE REQUIREMENTS
FOR
THE DEGREE OF MASTER OF SCIENCE
IN
METALLURGICAL AND MATERIALS ENGINEERING DEPARTMENT

AUGUST 2015

Approval of the thesis:

TRANSPARENT THIN FILM HEATERS
BASED ON SILVER NANOWIRE NETWORKS

Submitted by **ORÇUN ERGÜN** in partial fulfillment of the requirements for the degree of **Master of Science in Metallurgical and Materials Engineering Department, Middle East Technical University** by,

Prof. Dr. Gülbin Dural Ünver
Dean, Graduate School of **Natural and Applied Sciences** _____

Prof. Dr. C. Hakan Gür
Head of Department, **Metallurgical and Materials Eng.Dept., METU** _____

Assoc. Prof. Dr. Hüsnü Emrah Ünalın
Supervisor, **Metallurgical and Materials Eng.Dept., METU** _____

Examining Committee Members:

Prof. Dr. Raşit Turan
Physics Dept., METU _____

Assoc. Prof. Dr. Emren Nalbant Esentürk
Chemistry Dept., METU _____

Assoc. Prof. Dr. Abdullah Ceylan
Physics Eng. Dept., Hacettepe Univ. _____

Assoc. Prof. Dr. Yunus Eren Kalay
Metallurgical and Materials Eng. Dept., METU _____

Assoc. Prof. Dr. Hüsnü Emrah Ünalın
Metallurgical and Materials Eng. Dept., METU _____

Date: 24. 08. 2015

I hereby declare that all information in this document has been obtained and presented in accordance with academic rules and ethical conduct. I also declare that, as required by these rules and conduct, I have fully cited and referenced all material and results that are not original to this work.

Name, Last Name: Orçun ERGÜN

Signature:

ABSTRACT

TRANSPARENT THIN FILM HEATERS BASED ON SILVER NANOWIRE NETWORKS

Ergün, Orçun

M. S., Department of Metallurgical and Materials Engineering

Supervisor: Assoc. Prof. Dr. Hüsnü Emrah Ünal

August 2015, 71 pages

Transparent thin film heaters are used in various de-fogging and de-icing applications because of their ability to convert electrical energy to thermal energy while allowing to transmit solar light through a surface. Indium tin oxide (ITO) is the conventional transparent conducting material used in transparent thin film heaters. However, due to scarcity of indium and its increasing prices worldwide, coupled with the inflexibility of ITO, alternative materials are being investigated.

Silver nanowire networks have a great potential to be used as transparent thermal thin film heaters because bulk silver has the highest electrical conductivity among other metals, which result in low sheet resistances. Moreover, silver nanowire thin film networks demonstrate high optical transparency with low sheet resistance. Diameter of silver nanowires are in the order of few tens of nanometers, which confines electrons to travel through one dimension that result in high thermal performance due to Joule heating. In addition, silver nanowire based transparent thin film heaters can be made flexible on polymeric substrates.

In this thesis, silver nanowire based transparent thin film heaters were fabricated on quartz, soda lime silicate glass, polyethylene terephthalate (PET) substrates. Nanowire networks were deposited through simple spray coating method. Thermal performance as well as optoelectronic characteristics of the networks were determined. It is concluded that silver nanowire based transparent thin film heaters demonstrate high thermal performance coupled with high optical transmittance.

Keywords: transparent thin film heaters, silver nanowires, spray coating.

ÖZ

GÜMÜŞ NANOTEL İNCE FİMLER İLE ŞEFFAF ISITICILAR

Ergün, Orçun

Yüksek Lisans, Metalürji ve Malzeme Mühendisliği Bölümü

Tez Yöneticisi: Doç. Dr. Hüsnü Emrah Ünalın

Ağustos 2015, 71 sayfa

Şeffaf ince film ısıtıcılar, bir yüzeyden güneş ışığının geçmesine izin verirken bu yüzeyde elektrik enerjisini ısı enerjisine dönüştürebilme özelliklerinden dolayı pek çok buğu ve buz giderme uygulamasında kullanılırlar. İndiyum kalay oksit (ITO), bu amaçla şeffaf ince film ısıtıcılarda en çok kullanılan şeffaf elektriksel iletken malzemedir. Ancak, indiyumun azlığı ve dünya çapında artan fiyatları, ITO'nun esnek olmama özelliğiyle birleştiğinden alternatif malzemeler araştırılmaktadır.

Gümüşün diğer metaller arasında en yüksek elektriksel iletkenliğe ve bu nedenle düşük yüzey dirençlerine sahip olması nedeniyle, gümüş nanoteller şeffaf ince film ısıtıcı olarak kullanılmada yüksek bir potansiyele sahiptir. Buna ek olarak, Gümüş nanotel ince filmler düşük yüzey direnciyle birlikte yüksek optik geçirgenlik sergiler. Gümüş nanotellerin bir kaç on nanometre olan çapları, elektronları bir boyuta hapsederek ilerlemelerine ve Joule ısınmasıyla yüksek ısıtma performansı sergilemelerine yol açar. Buna ek olarak, gümüş nanotelden yapılmış ince film ısıtıcılar, polimerik alttaşlar üzerinde esnek özelliğe sahip olarak üretilebilir.

Bu tez çalışmasında, gümüş nanotel ince filmlerden yapılı şeffaf ısıtıcılar, kuvarz, silika camı ve polietilen tereftalat (PET) altaşları üzerinde üretildi. Nanotel ağırları spreyle yöntemiyle kaplandı. Nanotel ağırlarının ısı performansını, optoelektronik karakteristikleriyle birlikte saptandı. Gümüş nanotel ince filmlerden yapılı şeffaf ısıtıcıların yüksek optik geçirgenlikle birlikte yüksek ısı performansına sahip olduğu sonucuna varılmıştır.

Anahtar Kelimeler: şeffaf ince film ısıtıcılar, gümüş nanoteller, spreyle kaplama.

To the memory of my beloved grandfather, Şerif Ali ERGÜN

ACKNOWLEDGEMENTS

I would like to express my gratitude to my supervisor Assoc. Prof. Dr. Hüsni Emrah ÜNALAN, for his guidance and encouragement during my studies. He is a true inspiration as a high achiever young scientist.

Thanks to Şahin COŞKUN for preparing silver nanowires and transparent film heaters. Without his invaluable help, solid guidance and patience with me, this thesis would have never been completed.

I also would like to express my gratitude to my employer, ASELSAN A.Ş. and “Radar, Electronic Warfare and Intelligence Systems” Sector’s head Oğuz ŞENER, my director Şebnem SAYGINER and my manager Ali LAFCI for allowing me to pursue my master’s degree, for their guidance in my academic endeavors and for allowing me to use thermal measurement equipment for this research. We would like to acknowledge the partial financial support provided by Arçelik A.Ş.

Murat MUTLUOL’s and Hüseyin YURDAKUL’s help in preparing TTFH samples, Halil İbrahim ATASOY’s help in IR thermal camera measurements, Uğur ETİZ and Murat PARLAK’s help in providing thermal measurement equipment, Selçuk ÖKSÜZ’s help in measurement setup preparation are all greatly appreciated.

I sincerely thank my office mate Burcu AKSOY. I learned a lot from her point of view in my scientific studies, in work-related topics and in my personal life. The time we shared together has been so much fun and full of unforgettable moments. She is a wonderful partner.

Special thanks to Zeynep KARACA for her support during my studies, which is kindly appreciated. I want to thank Elif Selen YÜCEL for her guidance during preparation of my thesis. Her kind attitude and smiling face at the workplace is always admired.

I thank Ali Sina ÖNDER, Erkut AYKUTLUĞ and Gökhan METAN for being with me at hard times and sharing my happy moments even if they are at the other side of the globe. They are like real brothers.

I would like to thank my grandmothers, my dear aunt Neshun KAVUTÇU, my uncles, Zatiye Abla, Önalp, Çebi & Taşbaşı families for a loving and supportive family environment.

I thank my fabulous parents for their belief in me and for their support through all my life. What I achieve belong to them. Their love and encouragement made this thesis possible.

Thanks to İdil for being the greatest sister in the world and my undisclosed best friend. Her strength to hold on under the most challenging conditions coupled with her fun attitude towards life has been and will always be an inspiration during my career and personal life.

And lastly, I deeply thank all people whose mission is to encourage others to follow their dreams and passions. One of them is William Ernest Henley, whose words in his famous poem “Invictus” give me the strength to pursue my dreams from now on with an increasing and everlasting courage that stands against any fear:

*“...It matters not how strait the gate,
How charged with punishments the scroll,
I am the master of my fate:
I am the captain of my soul.”*

TABLE OF CONTENTS

ABSTRACT.....	v
ÖZ.....	vii
ACKNOWLEDGEMENTS.....	x
TABLE OF CONTENTS.....	xii
LIST OF FIGURES.....	xv
LIST OF TABLES.....	xviii
LIST OF ABBREVIATIONS.....	xix
CHAPTERS	
1. INTRODUCTION	
1.1. Motivation for the Study.....	1
1.2. Transparent Conducting Materials Used in Transparent Thin Film Heaters	4
1.2.1. Metal Oxides.....	10
1.2.1.1. Indium Tin Oxide (ITO).....	12
1.2.1.2. Fluorine Doped Tin Oxide (FTO).....	15
1.2.1.3. Zinc Oxide (ZnO).....	15
1.2.2. Carbon Nanotubes (CNTs).....	16
1.2.3. Graphene.....	17
1.2.4. Metallic Nanowires.....	18
1.2.4.1. Silver Nanowires (Ag NWs).....	19
1.2.4.2. Gold Nanowires (Au NWs).....	19
1.2.5. Hybrid Materials.....	20
1.3. Silver Nanowire Thin Films.....	20
1.3.1. Percolation Theory and Optoelectronic Properties of Nanowires....	20
1.3.2. Joule Heating Mechanism of Nanowire Networks	22

1.3.3. Failure Mechanism of Silver Nanowire Networks due to Joule Heating	24
1.4. Ag NW Synthesis by the Polyol Method	24
1.5. Ag NW Transparent Thin Film Heater Fabrication by Spray Coating	28
2. EXPERIMENTAL.....	31
2.1. Networks of Ag NWs for the Fabrication of TTFHs.....	31
2.1.1. Ag NWs Synthesis.....	31
2.1.2. Deposition of Ag NW Thin Films onto Various Substrates by Spray Coating.....	33
2.1.3. Physical Vapor Deposition of Ag Contacts on Ag NW Networks.....	34
2.1.4. Electrical Wiring and Cable Bonding	36
2.2. Infrared Imaging and Thermal Mapping for the TTFH Devices.....	37
2.3. Thermal Measurements under Bias.....	38
2.4. Scanning Electron Microscopy Imaging.....	39
2.5. Sheet Resistance Measurements.....	40
2.6. Transparency Measurements.....	40
3. RESULTS AND DISCUSSION.....	41
3.1. Effect of Contact Geometry.....	41
3.1.1. IR Thermal Camera Temperature Mappings.....	41
3.2. Effect of Ag NW Thin Film Density.....	44
3.2.1. SEM Images.....	44
3.2.2. Transparency, Sheet Resistance and Nanowire Density.....	45
3.2.3. Thermal Measurements Under Bias.....	46
3.3. Effect of Bias Voltage.....	48
3.3.1. Effect of Incremental Increase in Voltage Applied.....	51
3.4. Effect of Repetitive Heating and Cooling Cycles	53
3.5. Long Term Stability of TTFHs.....	55
3.6. Reproducibility of the TTFH Characteristics	56
3.7. Flexibility.....	58

4. CONCLUSIONS AND FUTURE WORK.....	59
4.1. Summary of the Work.....	59
4.2. Future Work.....	61
REFERENCES.....	63

LIST OF FIGURES

Figure 1.1. A flexible transparent conducting Ag NW thin film on a polymeric substrate.....	2
Figure 1.2. A commercial Kapton flexible thin film heater.....	2
Figure 1.3. a) A silver nanowire based touch-screen panel (Cambrios ClearOhm), b) Structure of a touch-screen panel.....	5
Figure 1.4. Examples of various TCOs.....	11
Figure 1.5. Thermal response of solution-processed ITO nanoparticles based TTFHs at various bias conditions.....	14
Figure 1.6. Thermal response characteristics of ITO nanoparticle paste based microheaters at various bias conditions.....	15
Figure 1.7. Heating performance of MWCNT sheet heaters.....	17
Figure 1.8. Percolation theory explained through conductivity as a function of percentage of NW projection area to the sample area.....	21
Figure 1.9. Transparency versus sheet resistance for various TCMs.....	22
Figure 1.10. A schematic of the synthesis mechanism of Ag NWs via solution based polyol process.....	27
Figure 2.1. Ethanolic solution of Ag NWs following purification.....	32
Figure 2.2. Spray coating of Ag NWs onto substrates.....	33
Figure 2.3. A photo of (a) Ag NW thin film coated on quartz sample, (b) optical microscope image of this film.....	34
Figure 2.4. Optical images of the interface between Ag NWs and Ag thin films showing (a) a succesful wetting and (b) a failed wetting	35
Figure 2.5. Dimensions of substrate and Ag contacts utilized in this work.....	36
Figure 2.6. A photo showing the final structure of the fabricated TTFHs in this work.....	36

Figure 2.7. Thermal mapping in IR thermal camera setup.....37

Figure 2.8. Thermal measurement setup utilized in this work.....38

Figure 2.9. A photo showing how the temperature measurements were taken via thermocouples.....39

Figure 2.10. Two probe setup used for the measurement of sheet resistances of the thin films.....40

Figure 3.1. Thermal camera images showing the effect of contact geometry on temperature distribution.....42

Figure 3.2. Optical microscope images of Ag NW thin films at the contact interface in parallel contact geometry (a) before and (b) after bias voltage application.....43

Figure 3.3 SEM images of Ag NW networks on quartz substrates with different number of times spray coating cycles that are (a) 30, (b) 37 and (c) 45 times.....44

Figure 3.4. Optical transmittance spectra of samples with Ag NW densities of 0.5, (b) 0.6 and (c) 1.6 NW/ μm^246

Figure 3.5. Change in temperature as a function of time at an applied bias of 4 V for samples with NW densities of 0.5, 0.6 and 1.6 NW/ μm^2 . Heating and cooling rate as a function of time for the sample with NW density of 1.6 NW/ μm^2 is given at the inset.....47

Figure 3.6. Change in temperature as a function of time for various applied biases to samples with Ag NW densities of 0.5, (b) 0.6 and (c) 1.6 NW/ μm^249

Figure 3.7. SEM images of the failed Ag NW thin film sample with a NW density of 0.6 NW/ μm^251

Figure 3.8. Change in temperature as a function of time for incrementally increased applied biases to the sample with a NW density of 1.6 NW/ μm^252

Figure 3.9. Change in temperature as a function of time under repetitive heating (3 V) and cooling cycles for a TTFH with a NW density of 1.6 NW/ μm^253

Figure 3.10. Change in temperature as a function of time under repetitive heating (11 V) and cooling cycles for a TTFH with a NW density of 0.5 NW/ μm^254

Figure 3.11. Change in temperature as a function of time for a TTFH with a NW density of 1.6 NW/ μm^2 which is long term biased at 3V.....56

Figure 3.12. Change in temperature as a function of time for a TTFH with a NW density of $1.6 \text{ NW}/\mu\text{m}^2$. Results for (a) right after the fabrication of TTFH devices ($R_s = 4.3 \text{ } \Omega/\text{sq}$), and (b) after 50 days of storage ($R_s = 4.9 \text{ } \Omega/\text{sq}$), are plotted.....57

Figure 3.13. Thermal response characteristics of Ag NW networks coated on flexible PET substrates in straight and bended (concave and convex) configurations under an applied bias of 4 V.....58

LIST OF TABLES

Table 1.1. TTFH properties for various TCMs.....	6
Table 1.2. Electrical properties of common TCOs. Conductivities reported are for best-case polycrystalline films.....	11
Table 1.3. Hybrid transparent conducting materials.....	20
Table 1.4. Dissipated power change under a fixed applied bias across two points with varying resistances.....	23
Table 1.5. General guide to transparent conducting electrode fabrication	29
Table 3.1. Sheet resistance, transmittance values at 550 nm and respective NW densities of 30, 37 and 45 times spray coated samples	45
Table 3.2. Maximum temperature reached at 4 V bias for samples having NW densities of 0.5, 0.6 and 1.6 NW/ μm^2	47
Table 3.3. Thermal response characteristics at maximum achievable temperature of samples with Ag NW densities of 0.5, 0.6 and 1.6 NW/ μm^2	48

LIST OF ABBREVIATIONS

1 D	One Dimensional
2 D	Two Dimensional
3 D	Three Dimensional
A	Ampere
Å	Angstrom
Ag	Silver
Au	Gold
°C	degrees Celsius
CNT	Carbon Nanotube
CVD	Chemical Vapor Deposition
Cu	Copper
EG	Ethylene Glycol
et al.	et alii (and others)
FOM	Figure of Merit
FTO	Fluorine doped Tin Oxide
h	hour
IR	Infrared Spectroscopy
ITO	Indium Tin Oxide
i.e	id est (in essence)
LCD	Liquid Crystal Display
LED	Light Emitting Diode
m²	square meters
min	minute
mm	millimeter
mg	milligram
mL	milliliter

Ni	Nickel
nm	nanometer
NP	Nanoparticle
NW	Nanowire
PEN	Polyethylene naphthalate
PET	Polyethylene terephthalate
PVD	Physical Vapor Deposition
PVP	Polyvinyl Pyrrolidone
RGO	Reduced Graphene Oxide
R_s	Sheet Resistance
s	second
SEM	Scanning Electron Microscopy
T (or T%)	Optical Transmittance / Transparency
TCE	Transparent Conducting Electrode
TCM	Transparent Conducting Material
TCO	Transparent Conducting Oxide
TTFH	Transparent Thin Film Heater
UV	Ultraviolet
V	Volt
W	Watt

CHAPTER 1

INTRODUCTION

1.1. Motivation for the Study

Up until now, nearly every heating equipment involves highly resistive elements based on nichrome or kanthal. However, they can only be used as strips or wires with various lengths and diameters.¹

On the other hand, transparent thin film heaters (TTFHs) are electrically conducting thin film materials that are used to convert electrical energy into thermal energy on a surface through which transmission of visible light is intended.

TTFHs are used in applications such as outdoor panel displays, aviation, liquid crystal display (LCD) panels, window defrosters,² thermoacoustic speakers³ and thermochromic devices⁴. Although defrosting in civilian vehicles is the mostly known application of TTFHS, they were firstly used in World War II in order to defrost airplane windows, which permitted high-altitude bombing.⁵ In the near future, TTFHs can also play a role in other defense applications such as anti-fogging of transparent antennas, multimedia display on windshields, military optics (such as shields, night vision devices, aircraft canopies and rifle scopes)⁶, and de-icing of large RF equipment such as bridge antenna towers and radome systems.⁷

TTFHs can be made flexible heaters provided that the heating unit is applied on flexible substrates such as polymers. Flexibility is particularly important if the specific application requires heating on curved surfaces. Flexibility is an important

parameter for TTFH fabrication since conventional transparent conductor materials such as indium tin oxide (ITO) cracks on flexible substrates. Instead, metal nanowire networks, as will be proposed in this work, can be used for flexibility. A photo of a flexible transparent conducting silver (Ag) nanowire (NW) thin film is shown in Figure 1.1.⁸

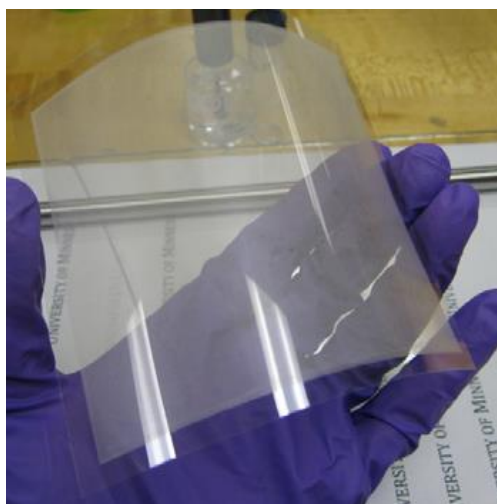


Figure 1.1. A flexible transparent conducting Ag NW thin film on a polymeric substrate.⁸

Flexible heaters that are not transparent are also used commercially as blood analyzers, anti-condensation units in helmets, electronic heaters, in medical diagnostics, telecommunications, defense and aerospace industries.⁹ A photo of a commercial Kapton non-transparent flexible thin film heater for the use of heating medical diagnostic equipment and satellite components is shown in Figure 1.2.¹⁰



Figure 1.2. A commercial Kapton flexible thin film heater.¹⁰

TTFHs should demonstrate high optical transmittance of at least 80 % in the visible region of the spectrum. In addition, they need to have low sheet resistance for high thermal efficiencies. Moreover, their transmittance and sheet resistance must be uniform over the whole electrode area. It is also required that they are stable for long term operation, can be processed easily, economically feasible to fabricate, and they must demonstrate high thermal stability.¹³

ITO is the conventional transparent conducting material used for TTFH applications.¹² It has advantages such as high optical transmittance and high electrical conductivity. However, it has some intrinsic disadvantages such as slow thermal response, degradation at high temperatures, requirements of high vacuum and high temperature for fabrication, incompatibility for flexible applications as discussed earlier, and instability in chemical media. In addition, since indium is a scarce and an expensive metal, there is an extensive research on the exploration of alternative materials.

Thin films with Ag NWs is one of the most important candidates due to high electrical conductivity of bulk Ag. Ag NWs also demonstrate high thermal performance because of the possible improved optoelectronic properties obtained at nanoscale due to dimensional effects, such as quantum confinement.

The purpose of this study is the fabrication and characterization of TTFHs using networks of Ag NWs. The objectives to achieve this goal are as follows:

- 1) Reproducibly depositing thin films of Ag NWs on different substrates such as quartz, soda lime silicate glass and polyethylene terephthalate (PET).
- 2) Fabricating TTFHs by depositing Ag contacts with appropriate geometry by thermal evaporation onto thin films of Ag NWs.
- 3) Optimizing thermal output of the films and transparency by understanding the effects of the following parameters: Ag contact geometry, density of Ag NWs

within thin film, value of applied bias, duration of applied bias, bending and failure mechanism of Ag NWs.

1.2. Transparent Conducting Materials Used in Transparent Thin Film Heaters

A “transparent conducting material (TCM)” is the term used to describe the active thin film material used in TTFHs that can simultaneously conduct electricity and transmit visible light. Optical transmittance (or transparency) denoted by T , and sheet resistance denoted by R_s are the two most important parameters⁵ that must be defined to evaluate a TTFH’s performance. Minimum standards required by industry for TCMs is that $T \geq 90\%$ and $R_s < 100 \Omega/\text{sq}$ as set by Hewlett-Packard (see ref [22] of Scardaci et al. 2011¹¹). A material’s possession of both of these properties is important because it is generally believed that high optical transparency is incompatible with high electronic conduction since optical transparency requires band gaps larger than 3.3 eV and such a large gap makes doping very difficult for semiconductors.¹²

Besides their use in TTFHs, TCMs are also used as electrodes in polymer solar cells, dye-sensitized solar cells, light emitting diodes, touch-screen panels and transparent capacitors.¹³ For example in an organic solar cell a TCM acts as either an anode or cathode, while letting solar light to pass through to allow generation of charge carriers within the solar cell.¹⁴ A commercial example of Ag NW thin film layer used as a TCM in a transparent touch-screen panel is given in Figure 1.3-a¹⁵, and the structure of the touch-screen panel is given in Figure 1.3-b¹⁶.

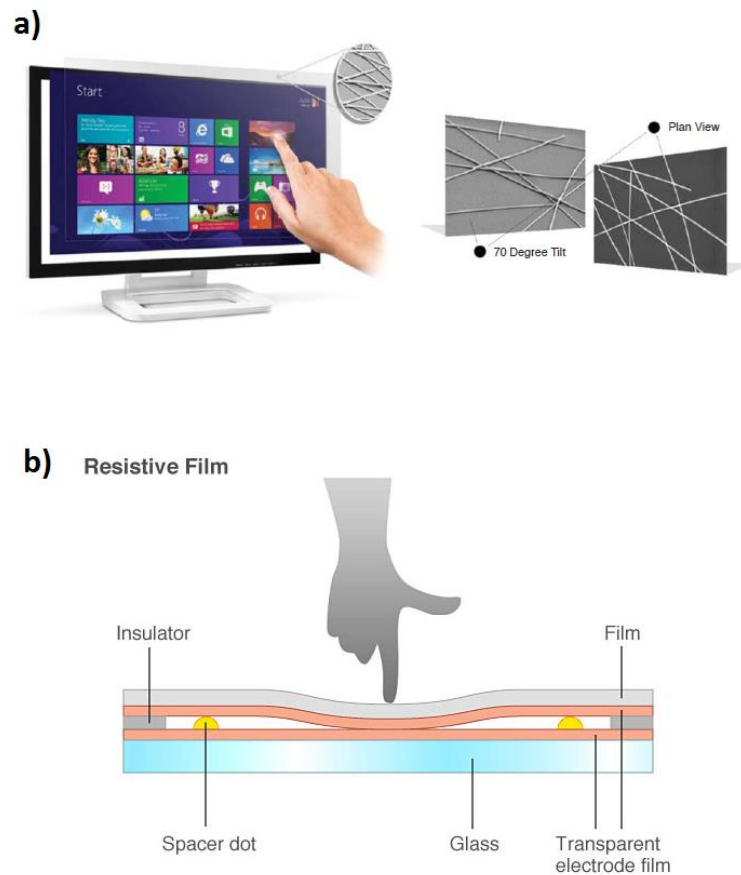


Figure 1.3. a) A silver nanowire based touch-screen panel (Cambrios ClearOhm)¹⁵, b) Structure of a touch-screen panel.¹⁶

An extensive literature review has been conducted on TTFHs and various properties of TCMs are tabulated in Table 1.1. Properties such as sheet resistance, transmittance, maximum temperature achieved under bias, voltage and current values at the maximum achieved temperature, and thermal resistivity values are compared within the table. This comparison serves as a general guideline to demonstrate where networks of Ag NW TTFHs stand in the current scientific research. A detailed analysis of each TCM (metal oxides, carbon nanotubes, graphene, metallic nanowires and hybrids of these materials) and their respective intrinsic properties are discussed in the following sections.

Table 1.1. TTFH properties for various TCMs.

Reference	Material	Synthesis Method	Substrate	Sample size (cm x cm)	Sheet Resist. R_s (Ω /sq)	Transmittance T, (%)	Max $T_{achieved}$ ($^{\circ}$ C)	Current at Max $T_{achieved}$ (A)	Bias at Max $T_{achieved}$ (V)	Input Power Density (W/cm^2)	Thermal Res. ($^{\circ}$ C. cm^2/W)
<i>This Study</i>	Ag NW	Polyol, spray coat.	Glass, Quartz	2.5 x 2.5	30	89	175	0.26	11	0.95	-
					25	88	180	0.33	9	0.99	-
					4.3	83	204	0.74	4	0.99	-
17	Ag wire mesh	Crack templ.	Glass	10 x 8	1	77	177	-	9	0.56	255
18	Ag mesh & ITO hybrid		PET**	3 x 4	300	88	43	0.65	12	0.65	-
4	Ag NW	Soln, Spray coat.	Glass, PEN**	2.5 x 2.5	35	85	55	-	7	0.24	121
19	Ag NW with clay platelets	Wet coat.	PET	5.0 x 7.5	10	90	100	-	7	-	-
20	Ag wire, crackle precursor	Vac.evap., spray coat.	PET, Glass tube	4 x 3 4 x 2	6	86	97	-	5	0.12	515
					2	70	92	-	2.25	0.17	409
21	Ag NW	Vacuum filtrating	PET, Quartz	2.5 x 2.5	11	92	138	-	7	-	-
22	Ag NW with RGO** sheets	Solvo-thermal	Quartz	2.5 x 2.5	27	80	225	-	15	-	-
23	Ag NW & CNT** hybrid	Spray coat., roll-to-roll	PET	4 x 4	-	-	110	-	15	-	-
							70	-	10	-	-
							40	-	5	0.017	-

Table 1.1. Continued.

Reference	Material	Synthesis Method	Substrate	Sample size (cm x cm)	Sheet Resist. R _s (Ω/sq)	Transmittance T _s (%)	Max T _{achieved} (°C)	Current at Max T _{achieved} (A)	Bias at Max T _{achieved} (V)	Input Power Density (W/cm ²)	Thermal Res. (°C.cm ² /W)
24	Ag NWs with ITO blankets	Spin coat	Polyimide	3 x 3	55	90	130	-	15	-	-
					50	85	105	-	12		
					45	96	80	-	9		
2	Ag NW in heat resistant polymer film	Drop cast	Polymer film	2.5 x 4.0	10	80	230	-	13	-	-
25	Ag NW / PEDOT:PSS polymer film	Spin coat / blading	Glass, PET	5 x 6	4	70	110	-	6	-	-
							90	-	4		
							55	-	3		
26	*Ag NW cloth, CNT cloth	Poyol, dip coat	Textile	2.54 x 2.54	-	0	52	-	1.2	-	-
							55	-	16		
27	Au wire network	Crack template	Quartz	2.5 x 2.5	5.4	87	600	5x10 ⁵ A/cm ²	15	4.2	139 (for 220 nm thick Au wires)
28	*CNT film aerogel	CVD, densific.	Aerogel	1.5 x 4.0	-	NA*	400	-	-	1.33	-
29	CNT film (multi-walled)		Glass, PET	0.6 x 0.85 (single sheet)	699	83	77	0.020	15	0.36	-
				1.3 x 0.9 (double sheet)	349	71	58	0.017	10	0.14	-

Table 1.1. Continued.

Reference	Material	Synthesis Method	Substrate	Sample size (cm x cm)	Sheet Resist. R_s (Ω /sq)	Transmittance T, (%)	Max $T_{achieved}$ ($^{\circ}$ C)	Current at Max $T_{achieved}$ (A)	Bias at Max $T_{achieved}$ (V)	Input Power Density (W/cm ²)	Thermal Res. ($^{\circ}$ C.cm ² /W)
30	CNT film (multi-walled)	e-beam	Glass	5-layer	172	48	140	-	40	-	-
				3-layer	342	67	116	-	40	-	-
				1-layer	756	87	100	-	40	-	-
31	CNT film (single-walled)	Dip coating	Glass	2 x 1	22.6 K Ω	96	48	-	60	0.24	90
					35.8 K Ω	98	41	-	60	0.15	105
					54.6 K Ω	98	38	-	60	0.09	137
32	CNT film (single-walled)	Spray coating	Glass	2.5 x 2.5	1190	91	210	-	12	0.12	-
33											
34	*CNT film (double-walled)	CVD	Glass	6 x 5	-	NA*	82	1.5	12	2.06	-
35	CNT film (single-walled)	Arc disch., vac. filtr.	Glass PET	4 x 4	356	76	95	-	12	-	-
36	Graphene	CVD	Glass	2 x 2	66	90	110	-	12	0.14	-
37	Graphene	CVD	PET	4 x 4	43	89	100	-	12	0.20	-

Table 1.1. Continued

Reference	Material	Synthesis Method	Substrate	Sample size (cm x cm)	Sheet Resist. R_s , (Ω /sq)	Transmittance T, (%)	Max $T_{achieved}$ ($^{\circ}$ C)	Current at Max $T_{achieved}$ (A)	Bias at Max $T_{achieved}$ (V)	Input Power Density (W/cm ²)	Thermal Res. ($^{\circ}$ C.cm ² /W)
38	Graphene	CVD	Glass, polymer	1 x 1	750	85	80	-	40	-	-
39	Graphene oxide	Soln. coat.	Flexible glass	10 x 20	5370	45	-	-	-	-	-
40	ITO nanoparticles	Solution processed, spin coated	Glass	-	633	≥ 90	163	-	20	2W	-
					763	≥ 90	100	-	15		
					3636	≥ 90	70	-	10		
41	*ITO nanoparticle paste film	Spin coat.	Quartz	1 x 1	23.5	NA*	445	-	12	-	-
42	ZnO (Ga doped) thin films	Pulsed laser dep.	Glass	1.25 x 1.25	2.14 $\times 10^{-4}$ Ω .cm	~ 90	88	-	12	-	-
							120	-	15		
							160	-	20		
43	ZnO (Ga doped) thin films	RF magnetron	Glass	1.25 x 1.25	90	-	42	-	-	90	-
44	Ag NW – copolymer composite film	Drop cast.	Self standing	4 x 1	25	~ 80	230	-	13	-	-

* Fabricated heaters in these studies are not transparent.

** RGO stands for reduced graphene, CNT stands for carbon nanotube, PET stands for polyethylene terephthalate, PEN stands for polyethylene naphthalate.

It is seen from Table 1.1 that Ag NWs display a high potential to be used as an alternative material to ITO in TTFHs. Ag NW based TTFHs fabricated in this study can reach temperatures higher than 175 °C with transmittances higher than 83 % under applied potentials lower than 12 V. These results compare well with other TTFH materials. There are only few studies that show similar or better thermal performances having comparable transmittances under similar applied voltages. One of these studies involves gold (Au) wire network TTFHs that can reach temperatures up to 600 °C with transmittances 87 % under an applied potential of 15 V.²⁷ This result has not been confirmed by another group. Another study involves single-walled carbon nanotubes that can reach temperatures up to 210 °C with transmittances 91 % under an applied potential of 12 V.^{32,33} Another study involves Ag NW-copolymer composite TTFH that can reach temperatures up to 230 °C with a transmittance between 78.5 to 81% and a sheet resistance of 25 Ω/sq under an applied potential of 13 V.

1.2.1. Metal Oxides

Some metal oxides belong to the family of transparent conducting oxide (TCO) materials with large band gaps (optical transparency requires band gaps larger than 3.3 eV)¹² in most cases.

TCOs are n-type semiconductors in which defects such as oxygen vacancies, impurity substitutions and interstitial atoms in the lattice donate their electrons to the conduction band providing charge carriers for the transport of electric current.^{45,46} Therefore, conductivity in n-type TCOs (and generally in other n-type semiconductors) is a consequence of electron transport.

Most common TCOs are indium oxide (In_2O_3), tin oxide (SnO_2) and zinc oxide (ZnO). Practical thin film transparent electrode applications utilize combinations of these oxides, which are shown in Figure 1.4.⁴⁷

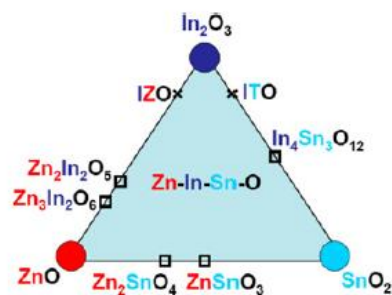


Figure 1.4. Examples of various TCOs.⁴⁷

Both In_2O_3 and SnO_2 are weak n-type semiconductors. Their charge carrier concentration and thus, the electrical conductivity can be increased significantly by extrinsic dopants, which is highly desirable.⁴⁸ Electrical properties of In_2O_3 , SnO_2 and ZnO are provided in Table 1.2.⁴⁹

Table 1.2. Electrical properties of common TCOs. Conductivities reported are for best-case polycrystalline films.⁴⁹

Material	Band gap (eV)	Conductivity (S/cm)	Electron concentration (cm^{-3})	Mobility ($\text{cm}^2/\text{V.s}$)
In_2O_3	3.75	10000	$>10^{21}$	35
SnO_2	3.35	8000	$>10^{21}$	20
ZnO	3.6	5000	$>10^{20}$	15

Although In_2O_3 , SnO_2 and ZnO have sufficient conductivities from the perspective of semiconductors, they are actually very poor conductors compared to metals.⁴⁹ For example the conductivities of silver (Ag), copper (Cu) and gold (Au) are 621000,

585000 and 442000 S/cm respectively.⁵⁰ Therefore, we can conclude that even the highest TCO conductivity is about a factor of 60 lower than that of the best conducting metal, Ag. This is one of the reasons why thin films of Ag NWs can be a good alternative to TCOs in TTFH and other transparent electronics applications. The theoretical absolute limit of the conductivity for a TCO has been estimated to be 25000 S/cm.⁵¹

There are also p-type TCOs. First one to be explored was CuAlO₂.^{49,52} Some of the other p-type TCO materials include nickel(II) oxide (NiO), potassium doped strontium copper oxide (SrCu₂O₂:K), indium(III) oxide-silver(I) oxide (In₂O₃-Ag₂O), calcium doped copper indium oxide (CuInO₂:Ca), copper scandium oxide (CuScO₂:O) and magnesium doped copper scandium oxide (CuScO₂:Mg).⁴⁹

P-type TCOs have very low conductivities with respect to n-type counterparts and they generally have low optical transmittance. To a large extent, the poor conductivity of p-type TCOs is due to the very low mobility of these materials, typically less than ~1 cm²/V.s, compared to mobilities of n-type TCOs (~10-40 cm²/V.s, as shown in Table 1.2).⁴⁹

1.2.1.1. Indium Tin Oxide (ITO)

Doped metal oxides, in particular ITO, or tin doped indium(III) oxide (In₂O₃:Sn), is the conventional and the most important TCM for almost four decades. The first study on ITO as a transparent conductive oxide was done in 1954.⁵³ ITO on glass is used as a transparent electrode in nearly all flat panel displays, and this application represents the largest economic value in TCM thin film coatings industry. The other major application of TCO is the low-emissivity (low-e) coatings for energy efficient windows.¹²

Rather than being Sn-doped In_2O_3 , ITO is really an In_2O_3 rich compound of In_2O_3 and SnO_2 as shown in Figure 1.4. In_2O_3 is a semiconductor with a band gap of 2.9 eV, while SnO_2 is a semiconductor with a band gap of 3.62 eV at 298 K. Sputtered ITO, has a typical band gap of 3.8 eV.^{48,54} Sputtered ITO has been reported to possess a carrier concentration in the range of $14.6\text{-}18.9 \times 10^{20} \text{ cm}^{-3}$, mobility in the range $25.7\text{-}32.7 \text{ cm}^2/\text{V.s}$, resistivity of about $1.3 \times 10^{-4} \text{ }\Omega\text{.cm}$, and transmittance of $\geq 80\%$ in the visible region of spectrum.⁵⁴

Since ITO demonstrates the advantage of such a high optical transmittance between 80-95% in the visible portion of the spectrum and a high electrical conductivity, it can provide low sheet resistances between 10-1000 Ω/sq .⁵⁵

However, ITO has some intrinsic disadvantages such as a slow thermal response, it degenerates into oxygen deficient species when heated above 400 °C, it requires high vacuum and high temperatures for the deposition, it is not flexible enough and cracks under mechanical bending, it is unstable in acidic and basic environments.^{56,57,58} Moreover, In is a high cost and a scarce material that makes exploration for ITO alternatives economically feasible.⁴⁸

There are some patents for use of ITO as a TTFH, specifically in the transparent toaster application.^{59,60} It was claimed that ITO (or fluorine doped tin oxide (FTO)) thin film based transparent toasters can reach up to 400 °C temperatures with a high input power of 1100 W.

Solution-processed ITO nanoparticle based TTFHs are investigated as an alternative to conventional ITO TTFHs. Thermal responses of these ITO nanoparticle based TTFHs with respect to the applied voltage are provided in Figure 1.5. It is seen that these TTFHs may not be ideal for heating applications as they achieve a temperature of only about 80 °C under an applied potential of 12 V. This temperature might not be enough for many applications that require higher performance under a maximum

applied potential of 12 V.⁴ 12 V is the maximum targeted bias that is applicable in most defogging and de-icing applications, which is desired to result in temperatures in excess of 100 °C.

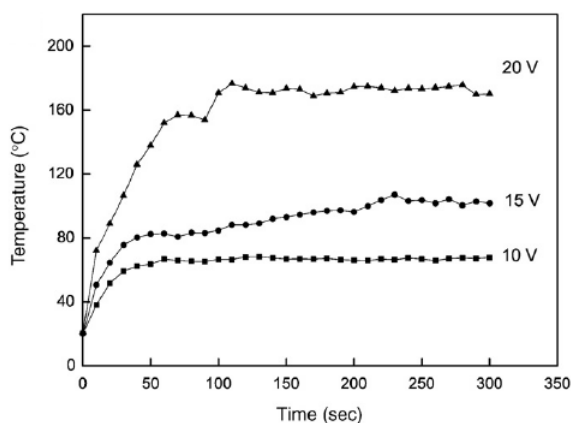


Figure 1.5. Thermal response of solution-processed ITO nanoparticles based TTFHs at various bias conditions.⁴⁰

In another study by Yang et al.⁴¹, ITO nanoparticle paste and organic additives are used to fabricate microheaters that can reach a maximum temperature of 400 °C at a bias of 12 V. Thermal response characteristics of these heaters are provided in Figure 1.6. However, these heaters were designed for microsensors and no transparency data was reported.

Because of the previously mentioned disadvantages of ITO, there is extensive research to develop ITO substitutes. There are some other metal oxide alternatives such as FTO, ZnO, along with other alternative materials such as carbon nanotubes, graphene, silver nanowires and hybrid materials. These ITO alternatives are discussed in the following sections.

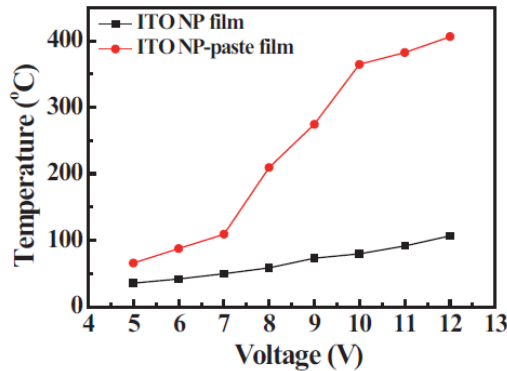


Figure 1.6. Thermal response characteristics of ITO nanoparticle paste based microheaters at various bias conditions.⁴¹

1.2.1.2. Fluorine Doped Tin Oxide (FTO)

FTO is the dominant material for SnO₂-based binary TCOs and the second widely used TCO. It has better thermal stability for TCE applications with respect to ITO⁶¹, it is cheaper, highly stable in hydrogen containing environments and it demonstrates better chemical stability. It is extensively used in dye-sensitized solar cells.⁴⁸ However, due to its average transparency (~80%), relatively low electrical conductivity⁶² and difficulties in fabrication it is not an ideal alternative to ITO in TTFH fabrication.⁴⁸

1.2.1.3. Zinc Oxide (ZnO)

Impurity doped ZnO (e.g., Ga- and Al- doped ZnO (GZO and AZO)) is nontoxic, abundant in earth's crust and economically viable that makes it a promising TCO material, alternative to ITO.^{63,43} AZO is the best candidate among impurity doped ZnOs from both the resources and the environmental points of view.⁴⁷ Both AZO and GZO have been shown to have low resistivity at high transparencies that gives

better performances than ITO in some cases.⁴⁸ Resistivity of AZO and GZO are reported as $\sim 8.5 \times 10^{-5} \text{ } \Omega/\text{cm}$ ⁶⁴ and $\sim 8.1 \times 10^{-5} \text{ } \Omega/\text{cm}$ ⁶⁵, respectively. These values are similar to the lowest reported resistivity of ITO that is $\sim 7.7 \times 10^{-5} \text{ } \Omega/\text{cm}$.⁶⁶ Resistivity of AZO and GZO also have better thermal stability than that of ITO.⁴⁸

Another advantage of AZO and GZO is their high optical transparency, which has typical values of 90% and above,⁴² comparable to that of ITO. Their high transparency stems from the wide band gap of the ZnO.⁴⁸

AZO and GZO also demonstrate better chemical stability at higher temperatures.^{67,68}

The disadvantage of AZO and GZO is that their mass production costs are high. New methods must be developed to mass produce these films over large areas at high growth rates with reliable properties.⁴⁸

1.2.2. Carbon Nanotubes (CNTs)

Carbon nanotubes are one-dimensional materials that are made up of carbon atoms in the form of rolled-up graphene. They can be single-walled (SWCNT) or multi-walled (MWCNT). After their discovery in 1991,⁶⁹ there have been extensive studies that demonstrate CNT's peculiar properties, which include high electrical conductivity of 10^6 S/m^2 (for SWCNTs)³⁵ and high thermal conductivity of 3500 W/m.K .³¹ However, as far as transparent conductive film applications are concerned, CNTs can not achieve the minimum standards set by industry ($T \geq 90\%$ and $R_s < 100 \text{ } \Omega/\text{sq}$, see ref [22] of Scardaci et al. 2011¹¹). A few examples on reported transparencies together with respective sheet resistances are 90% and $756 \text{ } \Omega/\text{sq}$ for MWCNTs³⁰, 79% and $580 \text{ } \Omega/\text{sq}$ for SWCNTs³², 70% and $130\text{-}190$ for SWCNTs³³, 85% and $1000 \text{ } \Omega/\text{sq}$ for SWCNT⁷⁰. The reason that higher transparencies result in

high sheet resistances in CNTs is the intertube contact resistances⁷¹ and presence of semiconducting SWCNTs.

Figure 1.7. shows TTFH performance of CNT thin films with 3 different sheet resistances. It is clear that these TTFHs need higher voltages than 12 V to reach targeted 100 °C.³⁰

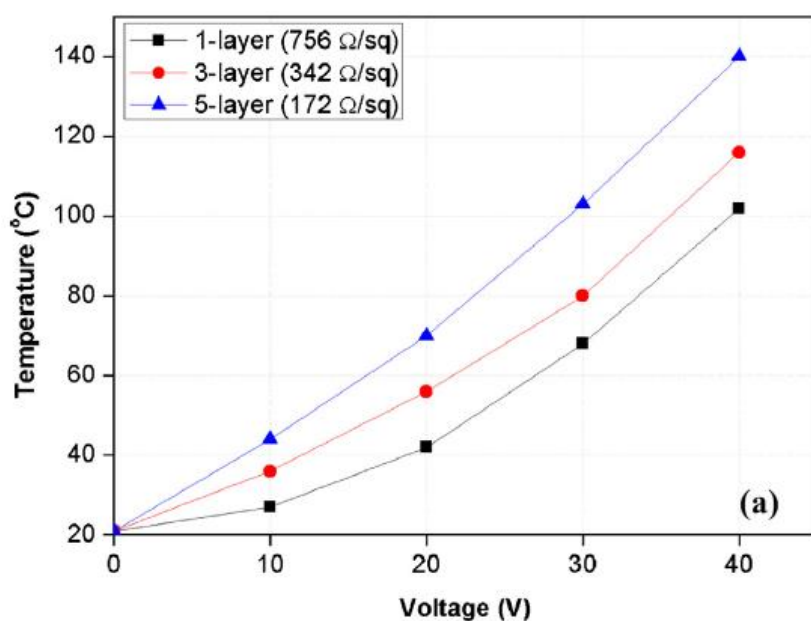


Figure 1.7. Heating performance of MWCNT sheet heaters.³⁰

1.2.3. Graphene

Graphene is a monolayer solely made up of carbon atoms that form a two dimensional hexagonal lattice with each atom at the vertex.⁷²

There are two seminal works on TTFH application of graphene. In terms of TTFH performance at an applied bias of 12 V, Bae et al. reported a T_{\max} of 110 °C (66

Ω/sq and 90% transparency)³⁶ and Kang et al. reported a T_{max} of 110 °C (43 Ω/sq and 89% transparency)³⁷. These studies both satisfy industrial requirements for TCEs, $T \geq 90\%$ and $R_s < 100 \Omega/\text{sq}$ as set by Hewlett-Packard (see ref [22] of Scardaci et al. 2011¹¹). However, they fail to show competitive heating performance.

1.2.4. Metallic Nanowires

Metallic nanowires have at least two dimensions between 1 and 100 nm. Due to their dimensions and confinement effects they have interesting optical, magnetic, electrical and thermal properties.⁷³

The most promising nanostructured material is probably Ag NWs¹¹ as they can be simply grown in solution and deposited from solution, are stable under flexing and networks of Ag NWs have low sheet resistances ($R_s < 100 \Omega/\text{sq}$) at high transparencies ($T \approx 85\%$). Due to their low optical conductivity, Ag NW networks display high optical transmittance for a given thickness.⁷⁴

In optical conduction, some of the photons passing through the material annihilate and lose their energy to excite the electrons within the material to the conduction band. So these electrons move across the material, forming an electrical current. Therefore low optical conductivity of a TCM is desired, because as lesser photons are annihilated higher optical transmittance is achieved.

Apart from Ag, the two most common metallic nanowires are Au and Cu. TTFH studies on Cu NWs are still in their infancy.

1.2.4.1. Silver Nanowires (Ag NWs)

Among metals, Ag has the highest thermal conductivity and the lowest electrical resistance, thus it is predominant candidate for the fabrication of TTFHs.⁴ Additionally, it is estimated that Ag NW thin films have a material cost of $\sim 30 \text{ \$/m}^2$ ¹¹ comparable to the cost of commercial ITO-coated glass⁷⁵. Ag NW synthesis is also easy, while large-scale synthesis of other metallic nanowires have not been reported so far.⁷⁶ Inherited from the intrinsic properties of Ag, networks of Ag NWs have advantages of high flexibility, high optical transmittance and high heating performance under low applied bias (generally below 12 V) that is of interest for many applications.⁴

In comparison to CNT thin films, thermal annealing of thin films of metallic nanowires cause a significant reduction in electrical resistance due to desorption of organic residues and sintering at the local junctions between the nanowires under constant optical transmittance. This is a major advantage of metallic nanowires against CNTs, which have high junction resistance between nanotubes as discussed earlier.⁷⁷

Moreover, Ag NW thin films display much higher figure of merits (direct current to optical conductivity ratio) than Ag thin films with similar thicknesses.⁷⁸

1.2.4.2. Gold Nanowires (Au NWs)

Au NWs are another type of metallic nanowires that may have a high potential for their use as TTFHs, since extraordinary optoelectronic properties have been reported solely by a group. A sheet resistance of 5.4 \Omega/sq has been reported at 87% transmittance (at 550 nm wavelength), with a maximum thermal response of $600 \text{ }^\circ\text{C}$.²⁷ However, these results are not confirmed or reproduced by another group.

1.2.5. Hybrid Materials

There are a number of studies that involve hybrid TCMs, few of which are provided with their properties in Table 1.3. Nanowire junctions increase the overall sheet resistance of the thin films. The driving force for the fabrication of hybrid materials is to decrease this junction resistance by the second material. Although not reported, these hybrid materials may have potential to be used as TTFHs.

Table 1.3. Hybrid transparent conducting materials.

Ref.	Hybrid TCM	Sheet Resistance ($\Omega/\text{sq.}$)	% Transmittance (550 nm)
79	Ag NW – Au NP – RGO	86	85
80	Ag NW mesh – Graphene	14	90
81	Ag NW – ITO	12	85
82	Ag NW – SnO	28	82
83	CNT – ITO	55	90
84	Cu NW – Ni NW	60	84

1.3. Silver Nanowire Thin Films

1.3.1. Percolation Theory and Optoelectronic Properties of Nanowires

Conduction in Ag NW networks can be described by “Percolation Theory” as explained schematically in Figure 1.8. Ag NWs tend to coalesce together more and more, and finally they reach a point called as “percolation threshold” (P_c) in which most of the NWs have formed intersections that can carry current through the network. Once NW density extends the percolation threshold, low sheet resistance can be obtained; however, this considerably reduces the transmittance.⁸⁵ Therefore, optimum conditions must be found without sacrificing either sheet resistance or

optical transmittance.⁸⁶ Another parameter that can affect P_c is the NW length. Using longer NWs shifts percolation threshold curve to left in Figure 1.8, meaning that samples with longer NWs display higher conductivity at lower percentage of NW projection area to the sample area.

In order to compare optoelectronic properties of different TCMs, one can define “Figure of Merit” (FoM), which is based on the considered physical properties. FoM is defined as ⁸⁷:

$$\text{FoM} = T^{10} / R_s$$

, where T is transparency at 550 nm, and R_s is sheet resistance of the film.⁷⁶

When FoMs of different TCMs are compared, as shown in the plot given in Figure 1.9., it is seen that the material whose FoM is closest to that of ITO is thin films of Ag NWs.⁷⁶

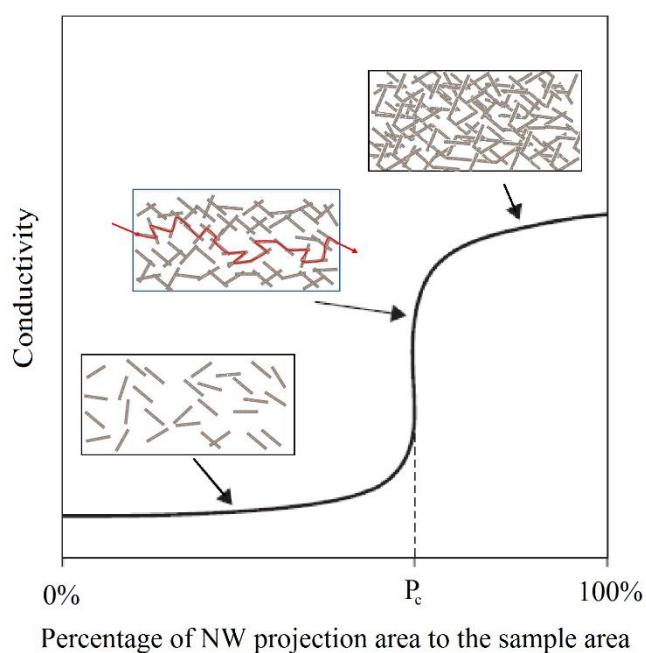


Figure 1.8. Percolation theory explained through conductivity as a function of percentage of NW projection area to the sample area.

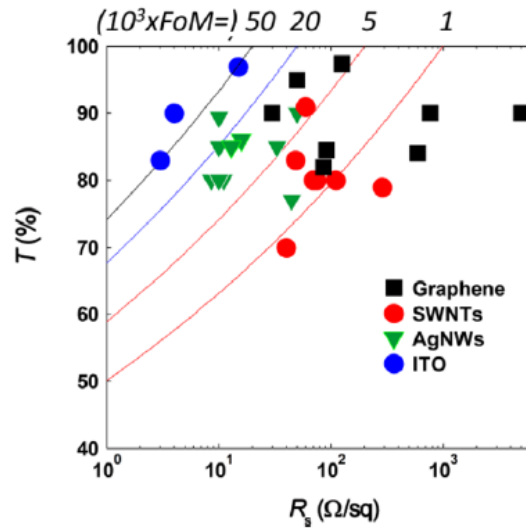


Figure 1.9. Transparency versus sheet resistance for various TCMs.⁷⁶

1.3.2. Joule Heating Mechanism of Nanowire Networks

TTFHs convert electrical energy into heat by the so-called “Joule Heating Mechanism”. Joule heating is the characteristic of a material that allows heating of a material when there is a current flow. As electrons flow through the material, electrical energy is transformed into thermal energy due to the partial loss of moving electrons’ energy to the vibration of the lattice phonons (vibrational modes of ions that make up the lattice).^{88,89} As the vibrational energy of lattice ions increases, temperature of the conducting body increases, allowing the TTFH to work as intended.

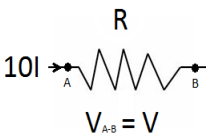
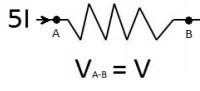
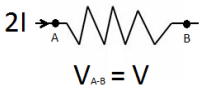
Power (P) converted from electrical energy to thermal energy can then be calculated by the following equation:

$$P = I \cdot V = I^2 \cdot R = \frac{V^2}{R}$$

, where I is the current through the resistor, R , and V is the voltage drop across the resistance.⁸⁸ This equation is valid for direct current (DC).

Example in Table 1.4 is provided to demonstrate how the dissipated power changes under a fixed applied bias across two points with varying resistances. As shown in the table, higher heat dissipation can be obtained at lower resistances for a fixed bias. This implies that utilizing thin films of metallic nanowires as TTFHs is advantageous since they have very low sheet resistances under high optical transmittance. Therefore, they can dissipate more power at a low applied bias.⁴

Table 1.4. Dissipated power change under a fixed applied bias across two points with varying resistances.

	1 st case	2 nd case	3 rd case
			
Applied bias (fixed)	V	V	V
Resistance	R	2 R	5 R
Current	10 I	5 I	2 I
Power dissipated	100 I ² R	50 I ² R	20 I ² R

The maximum steady-state temperature achieved in a TTFH is set by a balance between Joule heating and heat dissipation, which can be controlled by the applied bias.¹³ Increasing bias voltage decreases the mean free time of the electrons that result in an intensified scattering rate and more resistive losses due to optical phonon emission mechanism.⁹⁰

1.3.3. Failure Mechanism of Nanowire Networks due to Joule Heating

Current through a thin film of metallic nanowires travels within the nanowires, rather than uniformly distributed throughout the whole film. This great reduction in current flow area causes major increase in the current density, which in turn increases temperature sharply due to Joule heating. Therefore, Joule heating causes melting in the nanowire structure, which hinders performance of TTFHs. The network with higher sheet resistance will carry higher current density and it will fail more easily due to Joule heating.⁹¹

Moreover, metallic nanowires are known to have an energetic instability called “Rayleigh instability”. This is an important issue for the long-term reliability of the devices.⁷⁷ Rayleigh instability occurs due to the diffusion of surface atoms in a metallic NW. Surface diffusion results in the fragmentation of a NW into spherical fragments at temperatures much lower than the melting point of the parent metal and the metallic NW.⁹²

In addition, Joule heating also plays a role in a process called “electromigration” in which atoms in a device are displaced due to momentum transfer between charge carriers and the lattice⁹³. Electromigration is related to the transport of mass in metals when the metals are stressed at high current densities⁹⁴.

1.4. Ag NW Synthesis by the Polyol Method

Controlling size of the nanowires through synthesis is very crucial as the intrinsic electrical and optical properties of nanostructures are determined by their dimensions.⁷³ Since bulk Ag has a high thermal conductivity and the highest electrical conductivity among other metals, synthesis of Ag NWs is an active

research area, especially since 2013. Therefore, many synthesis methods have been developed to synthesize Ag NWs.

Ag NW synthesis methods include chemical synthesis,^{95,96} electrochemical technique,^{97,98} hydrothermal method,^{99,100} UV irradiation photodetection technique,^{101,102} DNA template,^{103,104} porous materials template,^{105,106} and polyol process.^{107,108} (references are taken from Coskun et al.¹⁰⁹). Vapor phase synthesis methods are mainly physical deposition methods, such as electron-beam deposition. On the other hand, because of the advantages of the nature of homogeneous reactions, wide range of solutions, simple monitoring technology and low cost, liquid phase synthesis methods are generally preferred.⁷³ Especially for the development of transparent flexible electrodes, synthesis of the required electrode materials using low-cost solution-based processes is one of the most important arguments.⁷⁶

When compared to other synthesis methods, the polyol approach appears as the most promising solution-based synthesis method due to its ease of mass production, cost and simplicity.⁷⁶ Polyol method involves production of the targeted metallic nanoparticles in colloidal form through reduction of inorganic salts by a polyol at mediocre temperatures.

Polyol synthesis was introduced by Fievet and co-workers for the synthesis of colloidal metallic nanoparticles such as Ag, Au, Cu, cobalt (Co), palladium (Pd), iridium (Ir), platinum (Pt), ruthenium (Ru), cobalt-nickel alloy (CoNi), and iron-nickel alloy (FeNi).^{110,111,112,113,114}

Xia et al. were first to successfully synthesize size- and shape-controlled single-crystal Ag nanoparticles along with other nanostructures using polyol process.¹¹⁵ After their work, metal nanostructures are widely synthesized by many research groups.⁷³ In this method, typically ethylene glycol (EG) is used as both the solvent

and the reducing agent, poly(vinylpyrrolidone) (PVP) is used as the stabilizing polymer (stabilizing agent), and silver nitrate (AgNO_3) is used as the Ag source.

In a slightly modified version of polyol process, a trace amount of a salt, such as sodium chloride (NaCl), iron(III) nitrate ($\text{Fe}(\text{NO}_3)_3$), copper(II) chloride (CuCl_2) or copper(I) chloride (CuCl) is added to the solution in order to control the morphology of the final products. This modified method is called as “salt-mediated polyol method”. Salt-mediated synthesis strategy is a simple and effective method, which is useful for the mass synthesis of Ag NWs.⁷³

In the polyol synthesis of Ag NWs¹⁰⁹, EG solution of PVP is prepared. NaCl is added to this solution. Solution is heated to elevated temperatures (optimum temperature is found to be $170\text{ }^\circ\text{C}$). AgNO_3 is added dropwise to EG+PVP+ NaCl solution under continuous stirring. With the introduction of Ag^+ ions into the solution, Ag nanoparticles start to form via homogeneous nucleation. Chemical adsorption of PVP molecules onto the surfaces of as-formed Ag nanoparticles is the reason for them to remain at nanoscale.¹¹⁶ As the process continues, some of the Ag nanoparticles start to dissolve and grow as larger nanoparticles via the mechanism known as Oswald ripening.¹¹⁷ With the passivation of some facets of these particles by PVP (stabilizing agent), some nanoparticles can grow into multitwin particles. PVP is believed to passivate (100) faces of these multitwin particles and leave (111) planes active for anisotropic growth at [110] direction. As the addition of Ag^+ ions continue, multitwin particles grow into Ag NWs. Final color of the growth solution indicates the formation of NWs. Following synthesis, centrifuging is carried out to purify the NWs by separating polymer and metallic by-products (nanoparticles etc.).

A schematic governing the synthesis mechanism of Ag NWs via solution based polyol process is provided in Figure 1.10.¹⁰⁹

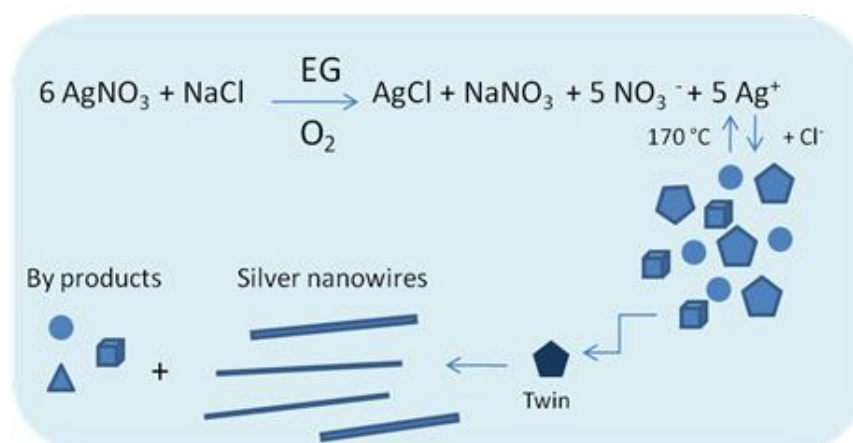


Figure 1.10. A schematic of the synthesis mechanism of Ag NWs via solution based polyol process.¹⁰⁹

Coskun et al.¹⁰⁹ found out that the temperature, AgNO_3 injection rate, PVP/ AgNO_3 (stabilizing agent/reducing agent) ratio, amount of NaCl added to the solution and stirring rate have important effects on the formation and dimensions of Ag NWs.

Following conclusions are drawn:

- Optimum polyol synthesis process temperature is 170°C . Below a certain temperature, high aspect ratio Ag NW formation is not possible. The length distribution of NWs widens beyond 170°C .
- AgNO_3 injection rate affects the final morphology of Ag nanostructures.
- Deficient and excess amounts of PVP over AgNO_3 result in the formation of undesired Ag structures in addition to nanowires.
- Absence of NaCl results in the formation of only Ag particles. the amount of NaCl that needs to be added to growth solution is $12 \mu\text{M}$. Beyond this optimum value, due to oversaturation, micrometersized Ag particles start to grow dominantly, suppressing Ag NW formation.
- Stirring rate affects the diameter and length of Ag NWs. As stirring is done faster, the diameter and length of the Ag NWs decrease.

As detailed in the Experimental section, optimum values of these parameters were used to synthesize Ag NWs for the fabrication of TTFHs in this thesis.

1.5. Ag NW Transparent Thin Film Heater Fabrication by Spray Coating

Achieving high reproducibility in deposition of colloidal solutions as thin films is often difficult.⁷⁶ Drop casting thin films of NWs exhibit inhomogeneities known as ‘coffee ring effect’ on the substrates during the solvent evaporation step.^{118,119} Films obtained through air-sprayed coatings are usually more homogeneous and tend to form much more uniform networks. In addition to this advantage, spray coating is also regarded as a fabrication method that is cheap, easy, conducted at low temperatures, compatible with various substrates and very suitable for scale-up.¹¹ It is also highly amenable to produce patterned films.¹²

Spray coating of Ag NWs onto substrates in order to form network Ag NW TTFHs involves pressure controlled spraying of nanowire suspensions by a spray gun onto the target substrate. Substrate is kept at an elevated temperature for instant removal of solvent through evaporation. Spray coated Ag NW thin films based transparent conducting films have been successfully achieved in many studies.^{120,121,4,11} Spray coating has also been used to deposit SWNT networks.^{122,123} In the case of heat sink applications, spray-coated Ag NWs on glass substrate are found to be well coupled to each other, thereby forming a continuous heat transfer pathway.¹²⁴ In the case of solar cell applications, depending on the experimental conditions used for their fabrication, thin films of metallic nanowires can have haze factors varying between 1 and 30%.¹²⁵ If low haze factor is desired, this can be achieved utilizing spray deposition, which can lead to haze factors below 2%. Such haziness is acceptable for display and window applications.⁷⁶

Different deposition routes for alternative TCMs are compared in Table 1.5.⁷⁶ As given in the table, spray coating (or spray deposition) is the best method for the fabrication of transparent conducting electrodes using Ag NWs.

Table 1.5. General guide to transparent conducting electrode fabrication.⁷⁶

Fabrication Method*	Ag NWs	TCOs	Graphene	CNTs
CVD	-	+++	+++	+
Sputtering	-	+++	-	-
Spin coating	++	-	+	++
Spray deposition	+++	++	+	+++
Screen printing	++	-	+	++
Cost	Medium	Low - High	High	High

* Fabrication method refers to the production of electrodes directly, not to the production of the constituent components which are used to fabricate the network.

CHAPTER 2

EXPERIMENTAL

2.1. Networks of Ag NWs for the Fabrication of TTFHs

2.1.1. Ag NWs Synthesis

For the synthesis of Ag NWs and their further purification including formation of NW suspensions, procedures reported by Coskun et al.¹⁰⁹ were followed.

All chemicals used in the synthesis procedure were purchased from Sigma Aldrich and used without further purification.

Prior to the synthesis, all glassware and substrates to be used in the experiments were cleaned. The cleaning procedure started with rinsing tools with deionized water. After that glasswares were washed with basic solution with pH 11, acidic solution with pH 2 and sonicated 10 minutes each within acetone (99.8%) and isopropyl alcohol (99.8%) baths. Finally, to get rid of chemical residues they were thoroughly rinsed with deionized water (with an electrical conductivity of 18.3 MΩ) and dried under nitrogen flow.

Following cleaning of the glassware, Ag NWs were synthesized through polyol process. For polyol process, 10 mL of 0.45M ethylene glycol solution of PVP (monomer-based calculation MW = 55 000) was prepared and 7 mg of 99.5% pure NaCl was added into this solution. The solution was heated at 170 °C in a two-necked round flask. 0.12 M AgNO₃ (99.5%) solution in 5 mL of EG was prepared

and added dropwise into the PVP solution by an injection pump (Top-5300 model syringe pump) at a rate of 5 mL/h. PVP:AgNO₃ molar ratio was 7.5 : 1. The solution was stirred at a rate of 1000 rpm by a magnetic stirrer during the whole process.

At the end of the synthesis, in order to separate polymer from the Ag NWs, the solution was diluted with acetone (in a ratio of 1:5) and centrifuged two times at 6000 rpm for 20 min. After that, NWs were dispersed in ethanol and again centrifuged at 6000 rpm for 20 min. A photo of ethanolic solution of Ag NWs following purification is given in Figure 2.1. Final solution color indicated the presence of Ag NWs. Ethanolic solution was used for the further deposition of Ag NW thin films via spray coating.

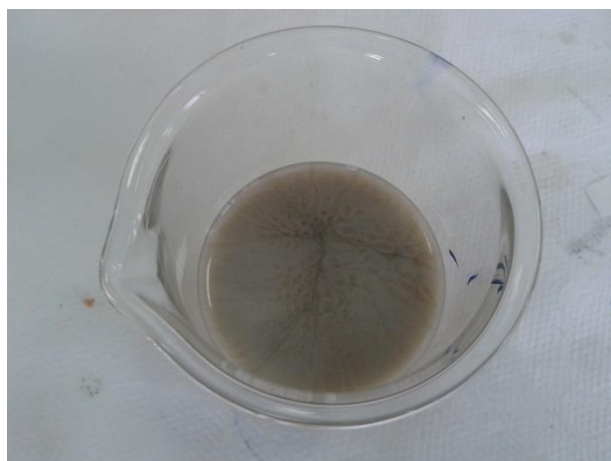


Figure 2.1. Ethanolic solution of Ag NWs following purification.

Typical diameter and length of the NWs synthesized in this work were 60 nm and 10 μ m on average, respectively. XRD peaks of the synthesized NWs in this study were shown to belong to pure silver (JCPDS Card No. 04-0783).¹²⁷

2.1.2. Deposition of Ag NW Thin Films onto Various Substrates by Spray Coating

A photo of the spray coating setup is provided in Figure 2.2. Ethanolic solution of Ag NWs were spray coated onto 2.5 cm x 2.5 cm substrates that were kept at 140 °C (by a hot plate) using a simple nitrogen fed air brush as shown in the figure.

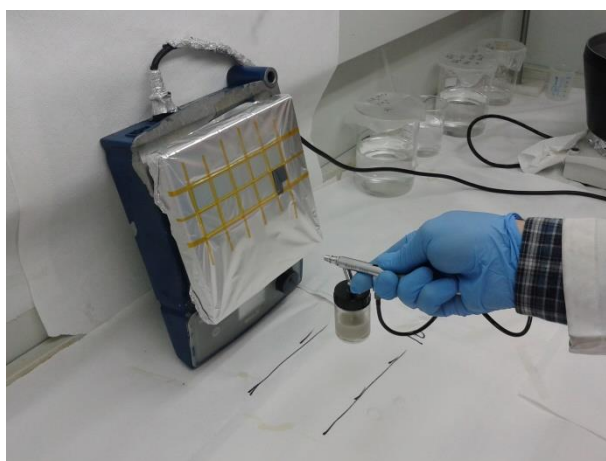


Figure 2.2. Spray coating of Ag NWs onto substrates.

Substrates used in this thesis include soda lime silicate glass, quartz and PET. The gas pressure and the distance between the air brush and the hot plate were effective parameters for the spray coating process. For reproducibility, the pressure and distance were set at 2 atm and 10 cm, respectively.

Following the spray coating process, thin films of Ag NWs were annealed at 200 °C for 20 minutes, in order to remove residual PVP that covers nanowires as an envelope and to decrease the contact resistance between Ag NWs at the junction points.¹²⁶

A photo of the quartz substrate with Ag NW thin film together with its optical microscope image is shown in Figure 2.3. Barely resolved Ag NWs are evident in the optical microscope image.

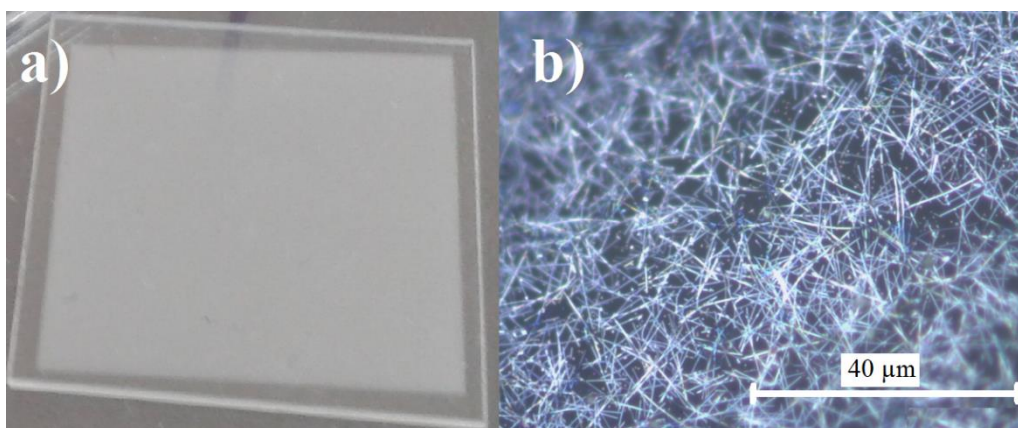


Figure 2.3. A photo of (a) Ag NW thin film coated on quartz sample, (b) optical microscope image of this film.

2.1.3. Physical Vapor Deposition of Ag Contacts on Ag NW Networks

Prior to the formation of Ag contacts by thermal evaporation, Ag NW network film coated substrates were masked using a shadow mask with the desired pattern. Equipment used in deposition of Ag thin films was Nanovak NVTH-350.

Ag deposition was not started until a base pressure of about 1.0×10^{-6} Torr was achieved. Pressure increased during deposition but never exceeded 1.0×10^{-5} Torr. Deposition was carried out at a current range of 45-60 A, voltage between 2.0-2.3 V and deposition rate between 1.5-2.0 Å/s. Deposition was finalized at a Ag thickness of 200 nm, monitored through a thickness monitor.

The interface between contact zone and Ag NW thin film is examined by the optical microscope images provided in Figure 2.4. Figure 2.4 (a) shows that the Ag NWs were wetted with Ag NW thin films; whereas Figure 2.4 (b) shows that the wetting was failed. The reason for failure as shown in the figure was the use of aluminum foil as the shadow mask in this sample. Following this, a proper mask was designed and got fabricated from a 1 mm thick aluminum plate and used for further experiments.

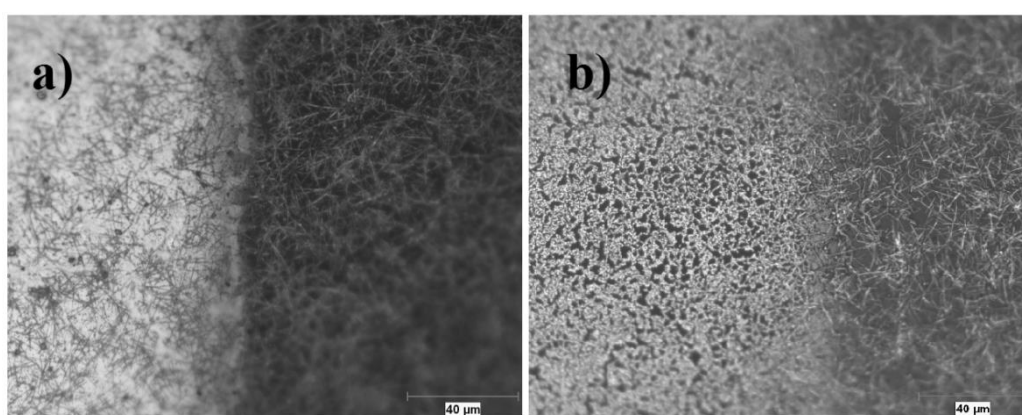


Figure 2.4. Optical images of the interface between Ag NWs and Ag thin films showing (a) a succesful wetting and (b) a failed wetting.

Dimensions of the Ag NW thin film deposited substrate and Ag contacts is given in Figure 2.5, defined by the shadow mask. Apart from this design, two other geometries were also investigated with no luck, as will be discussed in Chapter 3.

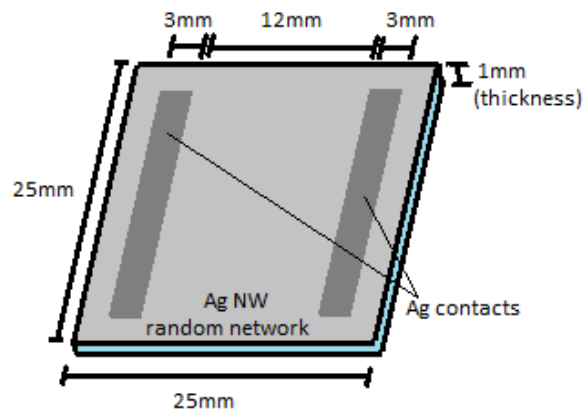


Figure 2.5. Dimensions of substrate and Ag contacts utilized in this work.

2.1.4. Electrical Wiring and Cable Bonding

Finally, electrical cables made of constantan were bonded to Ag contacts to finalize the TTFH fabrication. Bonding between endpoints of cables and Ag contacts were achieved by applying 2-component Ag filled epoxy (Elecolit 320H) followed by annealing at 100 °C for 1 hour. Final structure of the TTFH devices fabricated in this work is shown in the photo provided in Figure 2.6.

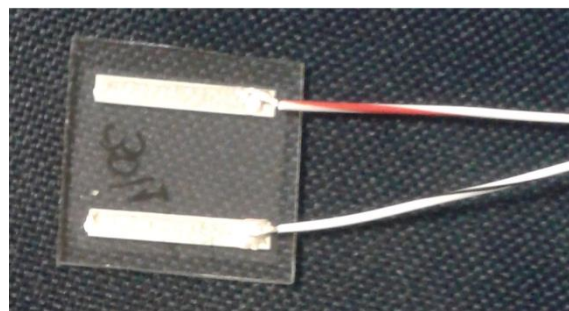


Figure 2.6. A photo showing the final structure of the fabricated TTFHs in this work.

2.2. Infrared Imaging and Thermal Mapping for the TTFH Devices

Infrared (IR) thermal measurements were done on a “QFI MWIR-512 InSb IR FPA Camera” equipped with “QFI MWIR-SE High Speed Thermal Transient Detector” with InfraScope™ MWIR Temperature Mapping InSb Focal Plane Array attachment.

Samples were attached on the camera’s aluminum plate that was held at 85 °C in order to heat the samples for achieving IR images that has enough contrast to be differentiated from background radiation. TTFH samples’ below surfaces were coated with a thermal grease (GC Electronics Type Z9 Heat Sink Compound) in order to achieve heat conduction between the plate and samples during measurements.

Electrical potential difference was applied between Ag contacts while IR camera detected and showed temperature distribution across the whole sample surface. A schematic on how temperature detection and thermal mapping was made for the TTFH samples is given in Figure 2.7.

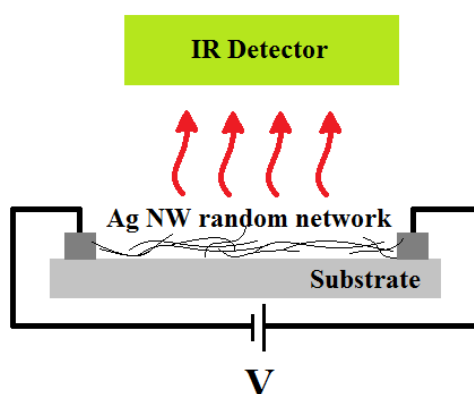


Figure 2.7. Thermal mapping in IR thermal camera setup.

Power was supplied through Ag contacts of TTFH samples by an Agilent 6032A system power supply unit. Either voltage or current was supplied through the unit.

2.3. Thermal Measurements under Bias

In addition to thermal imaging, performance of the TTFH samples under various applied potentials were investigated using a custom built setup, schematics of which is provided in Figure 2.8.

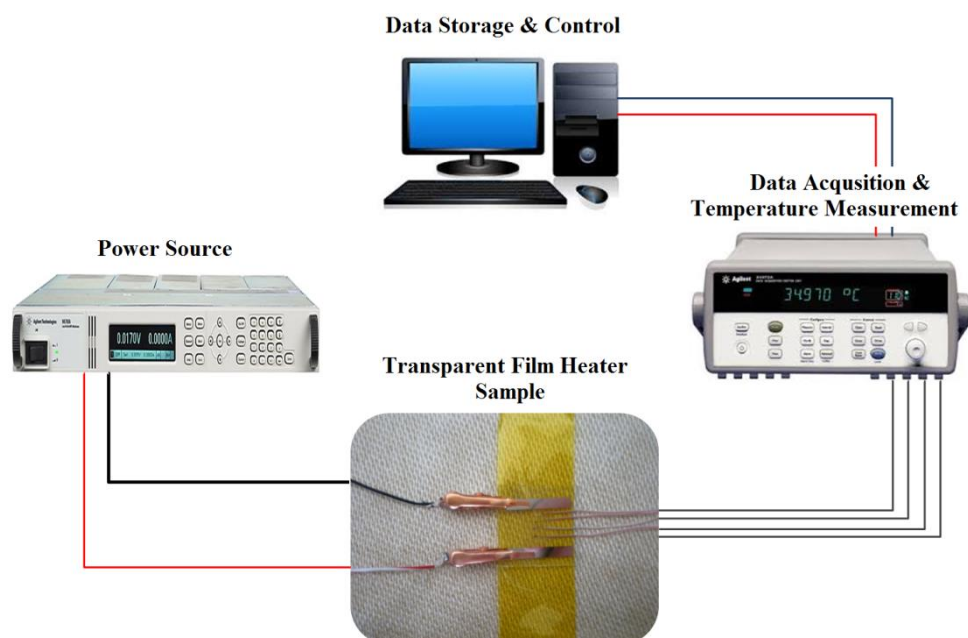


Figure 2.8. Thermal measurement setup utilized in this work.

Components of the setup include a power supply (Agilent 6032A system power supply unit, or Agilent N6744B DC power module attached to Agilent N6700B low profile MPS mainframe), a data acquisition unit (Agilent 34970A data acquisition/switch unit), a digital multimeter (Agilent 34401A) and a personal computer.

Temperature measurements were taken via 4 different fine wire thermocouples (J-type, iron-constantan) linked to the data acquisition unit. Thermocouples were attached to back surfaces of the TTFH samples by Kapton tape as shown in Figure 2.9.

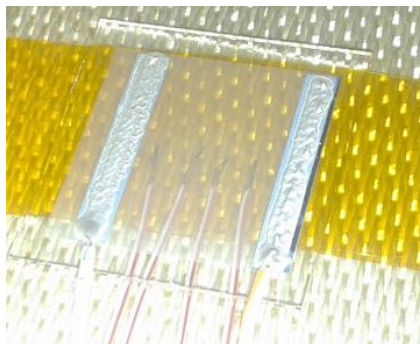


Figure 2.9. A photo showing how the temperature measurements were taken via thermocouples.

2.4. Scanning Electron Microscopy Imaging

Ag NW thin films were analyzed by Field Emission Scanning Electron Microscopy (FE-SEM) (Nova NanoSEM 430) operated at 10 kV voltage.

SEM images have been taken from the Ag NW thin films deposited on silicon wafers (p-type, single crystalline, 100 oriented). These wafers were placed next to other samples during spray coating of Ag NW thin films. Thus, the silicon samples and the TTFHs have identical NW densities. No further gold or carbon coating was utilized during imaging.

2.5. Sheet Resistance Measurements

Sheet resistance measurements were conducted by a two-probe setup which was able to measure R_s values accurately for the range involved.¹²⁷ During the measurements, a known current is sourced and it flows through an unknown resistance. A problem that occurs when using a 2-wire setup is that the voltage is measured not only across the resistance in question, but also includes the resistance of the leads and contacts. These parasitic resistances, however, are not creating a problem since the sheet resistances of the thin films were around a few ohms.

Sheet resistances of the samples were measured by 2-probe measurements, and a schematic of the setup is provided in Figure 2.10.¹²⁷

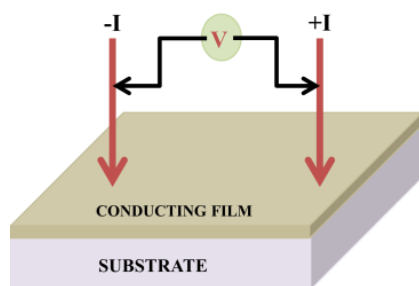


Figure 2.10. Two probe setup used for the measurement of sheet resistances of the thin films.¹²⁷

2.6. Transparency Measurements

The optical transmittance of Ag NW thin film samples were measured using a UV-VIS setup (Varian-Cary100 Bio) within the wavelength range of 300-800 nm at room temperature. In UV-VIS analyses, bare glass was used as the reference substrate for baseline correction. Although transmittance data is obtained as a spectra, for the sake of simplicity it is usually reported as a unique percentage value taken at a wavelength of 550 nm.

CHAPTER 3

RESULTS AND DISCUSSION

3.1. Effect of Contact Geometry

3.1.1. IR Thermal Camera Temperature Mappings

TTFHs with Ag NW networks on soda lime silicate glass substrates with 3 different contact geometries were fabricated. Temperature distribution of each sample under bias was monitored by the thermal camera. Obtained images with respect to the contact geometries are provided in Figure 3.1. (a), (b) and (c).

Device in Figure 3.1 (a) had parallel contact geometry. This sample could withstand temperatures up to 180 °C. Ag NW thin film was properly functioning when the sample failed due to cracking of the glass substrate at 180 °C (corresponding to an applied bias of 9.8 V and a resulting current of 2.3 A). As will be discussed, in Figure 3.2 no difference in the structure of Ag NW networks were observed following the application of bias.

Device in Figure 3.1 (b) had a 4-contact geometry. This sample could withstand temperatures around 120 °C (corresponding to an applied bias of 9.0 V and a resulting current of 2.0 A). Temperature at the corners were higher than 180 °C at the time of failure at 120 °C (mean sample temperature). The reason for the failure is melting of the Ag NWs at the corners due to high current and high temperature at the sharp edges of contacts as shown in the thermal image at the inset.

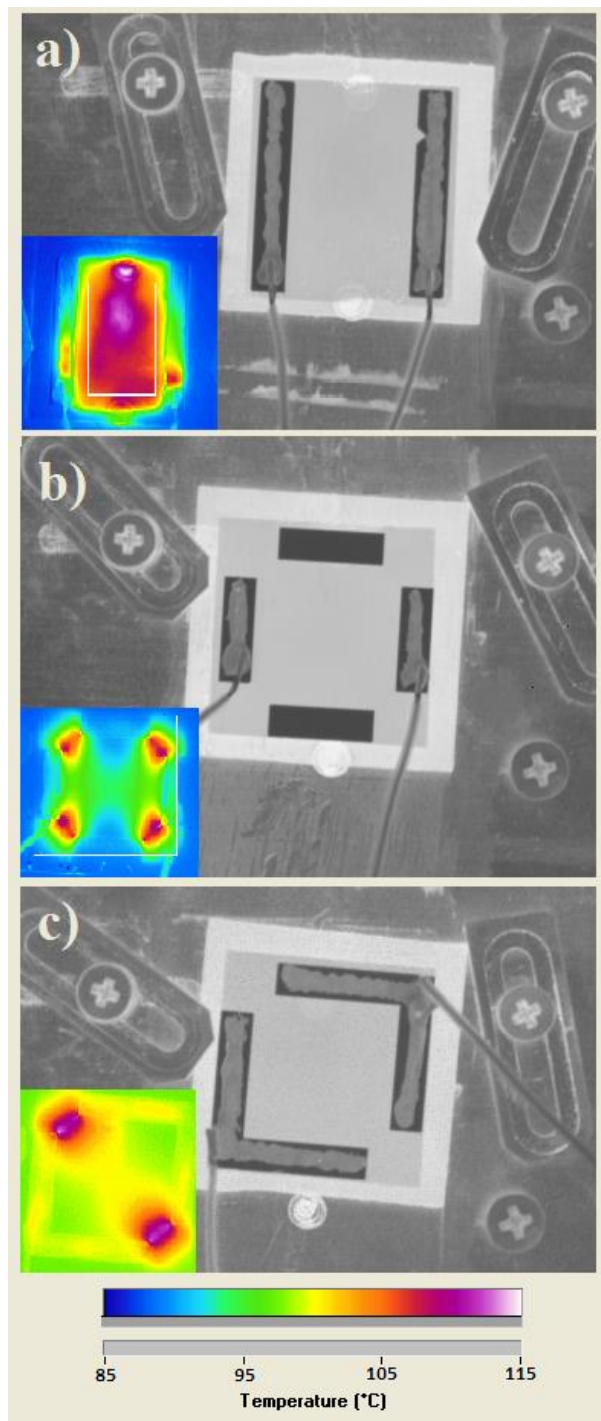


Figure 3.1. Thermal camera images showing the effect of contact geometry on temperature distribution. (a) Parallel contact geometry, (b) 4-contact geometry, and (c) opposite corners 2-contact geometry. Thermal images are provided at the insets.

Device in Figure 3.1 (c) on the other hand, had an “L” shaped 2-contact geometry at opposite corners. This sample could withstand temperatures around 110 °C (corresponding to an applied bias of 4.5 V and a resulting current of 2.2 A). Temperature at the corners were higher than 170 °C at the time of failure at 110 °C (mean sample temperature). Similar to the device in Figure 3.1 (b), the reason for the failure is melting of the Ag NWs at the corners due to high current and high temperature at the sharp edges of contacts as shown in the thermal image at the inset.

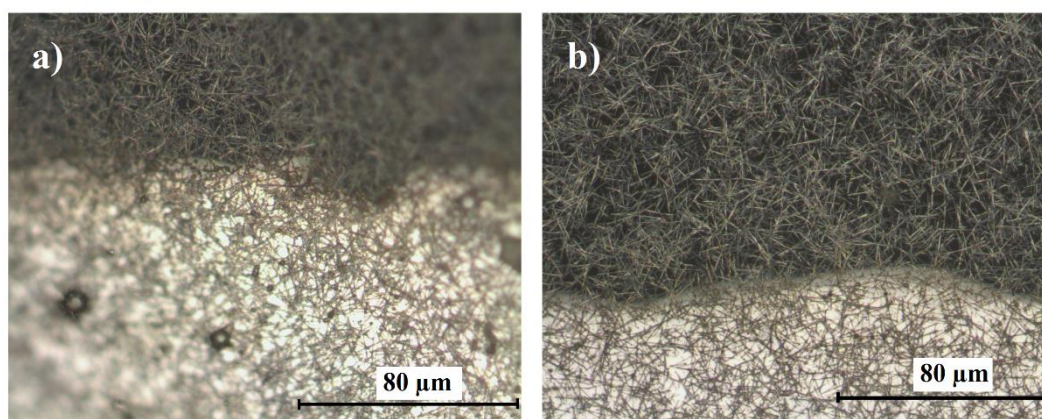


Figure 3.2. Optical microscope images of Ag NW thin films at the contact interface in parallel contact geometry (a) before and (b) after bias voltage application.

It is concluded that sharp corners having small distances in between, result in high electrical flux and must be avoided. Therefore, TTFHs having two parallel contacts on the opposite sides achieve the most homogeneous temperature distribution, withstand higher temperatures and currents before the failure of Ag NW networks.

It is also predicted that Ag NW networks can withstand temperatures higher than 180 °C provided that the substrate withstands to those temperatures without cracking.

3.2. Effect of Ag NW Thin Film Density

3.2.1. SEM Images

Ag NW network density has an important effect on the electrical conductivity as more contacts are formed at higher nanowire densities. Density of the nanowires can simply be increased through increasing number of spray coating cycles. The effect of the number of spray coating cycles on the nanowire density can be seen in the SEM images provided in Figure 3.3. SEM images in Figure 3.3 (a)-(c) correspond to Ag NW networks that are spray coated on quartz substrates for 30, 37 and 45 times, respectively.

The sample in Figure 3.3 (a) is spray coated the least number of times (30 times) and have the least nanowire density, thus, the least amount of contacts between nanowires. On the other hand, the sample in Figure 3.3 (c) is spray coated the most number of times (45 times) has the highest nanowire density, thus, the most number of nanowire contact points.

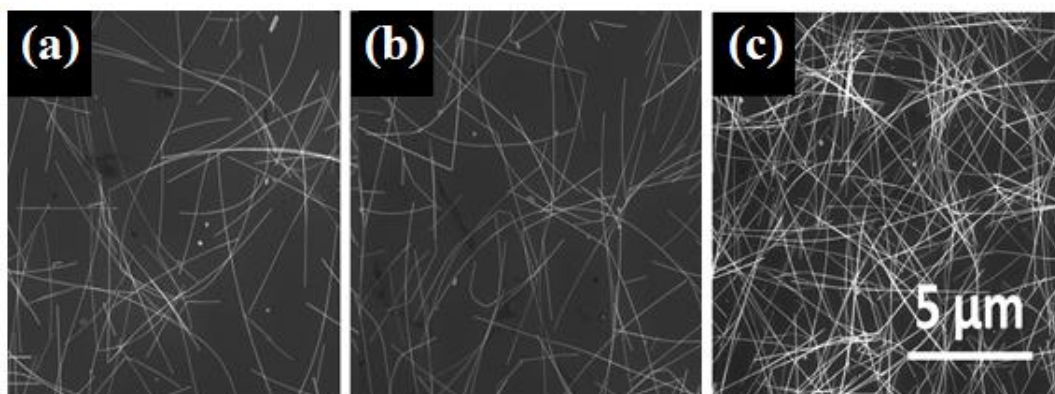


Figure 3.3. SEM images of Ag NW networks on quartz substrates with different number of times spray coating cycles that are (a) 30, (b) 37 and (c) 45 times. All scales are the same.

3.2.2. Transparency, Sheet Resistance and Nanowire Density

The transmittance values at 550 nm corresponding to different sheet resistances of Ag NW networks that are 30, 37 and 45 times coated on quartz substrates with their respective calculated NW densities are tabulated and provided in Table 3.1.

Table 3.1. Sheet resistance, transmittance values at 550 nm and respective NW densities of 30, 37 and 45 times spray coated samples.

Sample (# of times coated)	Sheet Resistance (Ω/sq)	Transmittance (550 nm) (%)	NW Density ($\text{NW}/\mu\text{m}^2$)
30	30	89.6	~ 0.5
37	25	88.3	~ 0.6
45	4.3	83.6	~ 1.6

As shown in Table 3.1, NW density values are interpolated according to sheet resistance values and the respective transmittances obtained in our group. Actual values are calculated from SEM images using ImageJ software (developed by Wayne Rasband).

It is concluded from Table 3.1 that as NW density is increased, number of NW contacts are increased, which in turn increases conductivity and reduces the sheet resistance. On the other hand, since there are more NWs per unit area in a denser sample, transparency is decreased due to higher absorption (or higher scattering) of light passing through the TTFH.

Optical transmittance spectra of samples with densities of 0.5, 0.6 and 1.6 $\text{NW}/\mu\text{m}^2$ are given in Figure 3.4.

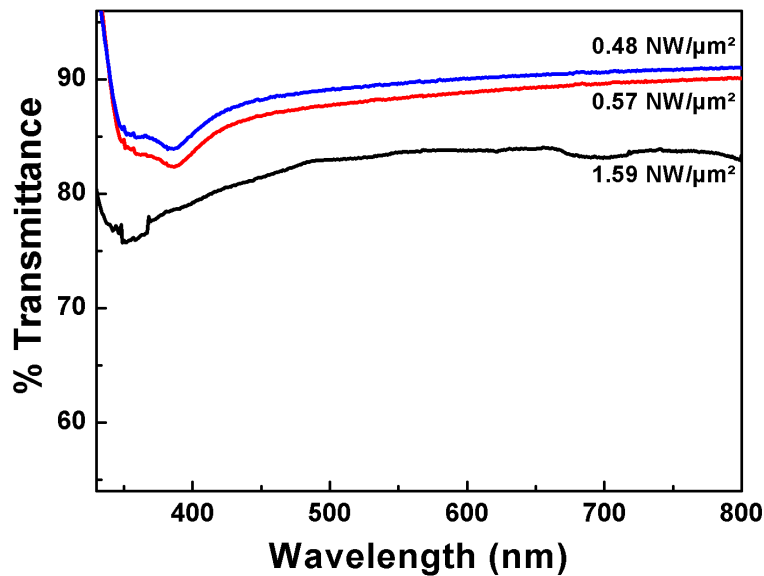


Figure 3.4. Optical transmittance spectra of samples with Ag NW densities of 0.5, (b) 0.6 and (c) 1.6 $\text{NW}/\mu\text{m}^2$.

3.2.3. Thermal Measurements Under Bias

Figure 3.5 shows the thermal behaviour of TTFHs with Ag NW thin films on quartz substrates with respect to time at an applied bias of 4 V for NW densities of 0.5, 0.6 and 1.6 $\text{NW}/\mu\text{m}^2$. Heating and cooling rate as a function of time for the sample having NW density of 1.6 $\text{NW}/\mu\text{m}^2$ is also given at the inset.

Attained maximum temperature values at an applied bias of 4 V at the end of 20 minutes of application of bias for 3 different nanowire densities are tabulated and provided in Table 3.2.

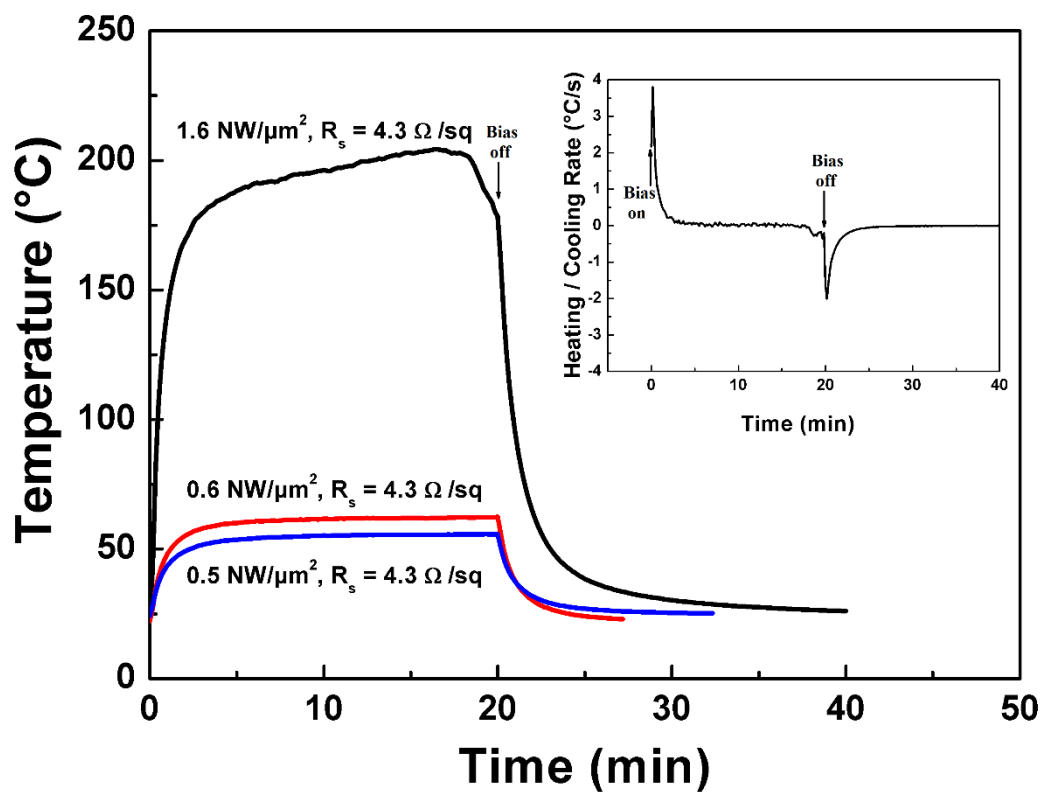


Figure 3.5. Change in temperature as a function of time at an applied bias of 4 V for samples with NW densities of 0.5, 0.6 and 1.6 $\text{NW}/\mu\text{m}^2$. Heating and cooling rate as a function of time for the sample with NW density of 1.6 $\text{NW}/\mu\text{m}^2$ is given at the inset.

Table 3.2. Maximum temperature reached at 4 V bias for samples with NW densities of 0.5, 0.6 and 1.6 $\text{NW}/\mu\text{m}^2$.

Sample (NW density - $\text{NW}/\mu\text{m}^2$)	R_s (Ω/sq)	Max. temperature achieved at 4 V bias
0.5	30	55
0.6	25	62
1.6	4.3	204

Table 3.2 clearly shows that TTFHs having higher nanowire densities (therefore lower sheet resistances) can reach higher maximum temperatures under the same applied bias. This is in consistency with the comment given for Table 1.4 that higher heat dissipation can be obtained for networks with lower sheet resistances under a fixed bias.

3.3. Effect of Bias Voltage

Effect of bias voltage on the temperature behaviour of TTFHs with Ag NW densities of 0.5, 0.6 and 1.6 NW/ μm^2 is given in Figure 3.6. Applied voltages and corresponding current values are marked on the curves. For these measurements, voltage was applied for 20 minutes and then it was turned off for another 20 minutes.

Achieved maximum temperature (T_{max}), in conjunction with the applied bias, corresponding current and calculated power densities are tabulated and provided in Table 3.3.

Table 3.3. Thermal response characteristics at maximum achievable temperature of samples with Ag NW densities of 0.5, 0.6 and 1.6 NW/ μm^2 .

Sample (NW/ μm^2)	Sheet Resistance (Ω/sq)	T_{max} achieved ($^{\circ}\text{C}$)	Bias at T_{max} (V)	Current at T_{max} (A)	Input Power Density* (W/ cm^2)
0.5	30	175	11	0.26	0.95
0.6	25	180	9	0.33	0.99
1.6	4.3	204**	4	0.74	0.99

* Effective sample area is taken as 3 cm^2 (with regard to dimensions of 2.5 cm x 1.2 cm, see Figure 2.5).

** Sample begins to lose stability after reaching a maximum temperature of 204 $^{\circ}\text{C}$ as seen from Figure 3.6.

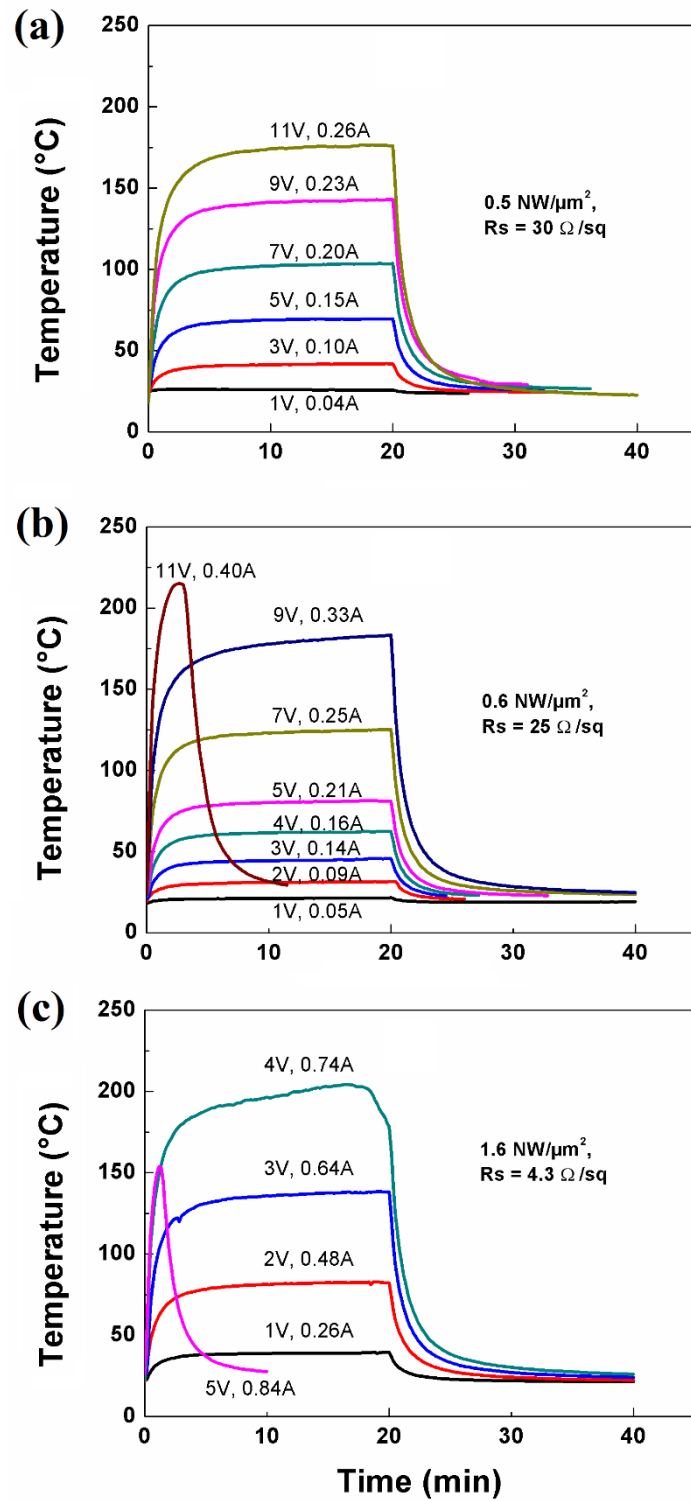


Figure 3.6. Change in temperature as a function of time for various applied biases to samples with NW densities of (a) 0.5, (b) 0.6 and (c) 1.6 NW/μm².

It is seen from Table 3.3 that the achieved maximum temperature is 204 °C under an applied potential of 4 V bias for the sample with Ag NW density of 1.6 NW/ μm^2 . However, this maximum temperature was not stable. The maximum stable temperature was 180 °C under an applied bias of 9 V for the sample with Ag NW density of 0.6 NW/ μm^2 . In addition to that, the sample with Ag NW density of 0.5 NW/ μm^2 reached a maximum temperature of 175 °C under an applied bias of 11 V. All Ag NW network samples' %T and R_s nearly meet the minimum standards required by industry for TCEs, $T \geq 90\%$ and $R_s < 100 \Omega/\text{sq}$ as set by Hewlett-Packard (see ref [22] of Scardaci et al. 2011¹¹). In addition, TTFHs fabricated in this study using Ag NW networks had high performance even below 12 V, which is the maximum bias voltage for many applications. When these values are compared with other TTFHs' performances (provided in Table 1.1), it is observed that only Au NW TTFH (with a sheet resistance of 5.4 Ω/sq , 87 % transmittance, and 600 °C maximum temperature) can outperform Ag NW TTFHs fabricated in this study.

SEM images of a failed Ag NW network is given in Figure 3.7 (a)-(d). These SEM images belong to the sample with Ag NW density of 0.6 NW/ μm^2 . They were obtained from the sample failed under the application of 11 V (whose thermal response characteristics is shown in Figure 3.6 (b)).

It is observed that, as the temperature increases with an applied potential of 11 V, Ag NWs begin to melt due to "Rayleigh instability" as discussed previously, and Ag begins to accumulate at nanowire junctions as observed in Figure 3.7 (a). Melting of thin Ag NWs results in Ag NWs getting even thinner as indicated in Figure 3.7 (b). As the temperature continues to increase, Ag NWs begin to fail and rupture as shown in Figure 3.7 (c). This results in a fewer current pathways, which begins to increase the sheet resistance of the networks upto kilohms and then megaohms. Finally, NWs break into discontinuous segments as shown in Figure 3.7 (d), TTFH fails and thermal response drops to zero.

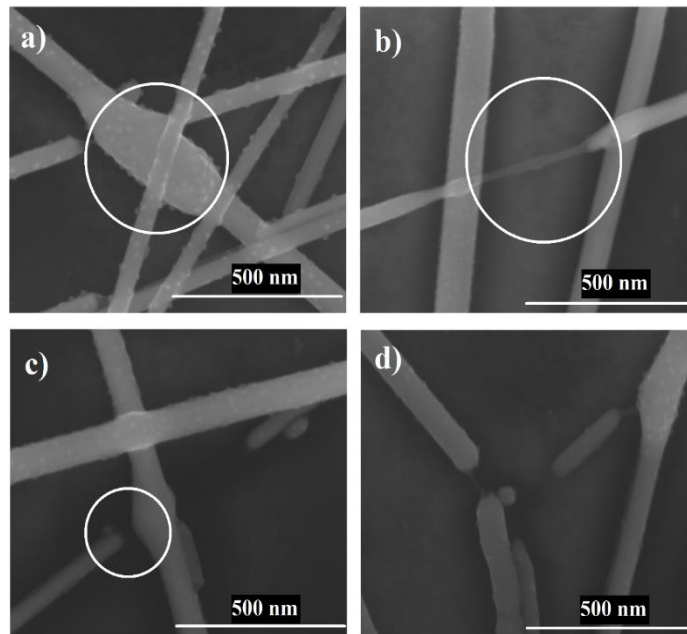


Figure 3.7. SEM images of the failed Ag NW network sample with a NW density of $0.6 \text{ NW}/\mu\text{m}^2$.

3.3.1. Effect of Incremental Increase in Voltage Applied

In the case of an incremental increase in the applied voltage, there occurs a subtle difference in the observed TTFH behaviour. This is depicted in Figure 3.8. For these measurements, voltage was gradually increased with steps of 0.5 V in every 10 minutes, until a final voltage of 5 V was reached.

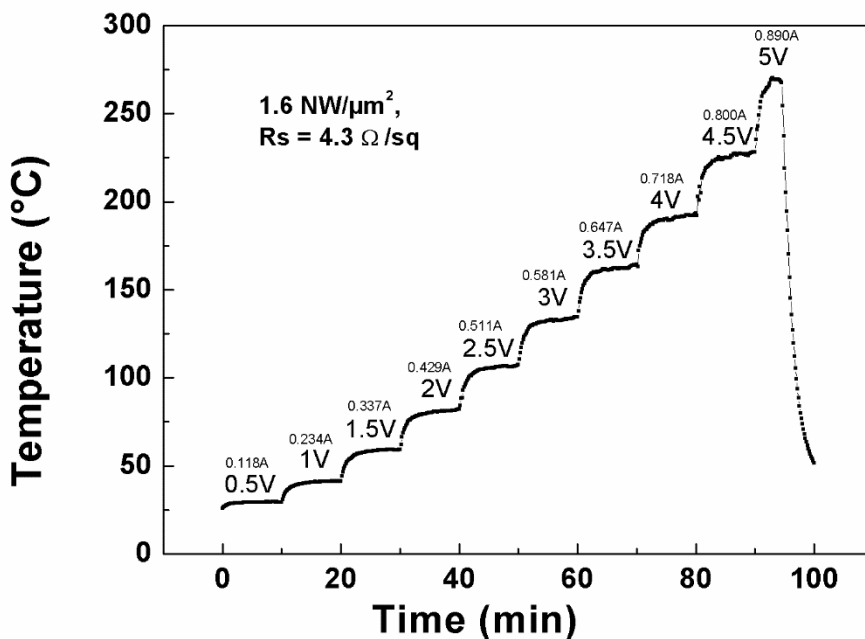


Figure 3.8. Change in temperature as a function of time for incrementally increased applied biases to the sample with a NW density of $1.6 \text{ NW}/\mu\text{m}^2$.

As seen from Figure 3.8, when the voltage is increased incrementally, Ag NWs can withstand higher applied bias and higher temperatures. It is known from Figure 3.6 (c) that the sample with a density of $1.6 \text{ NW}/\mu\text{m}^2$ could reach a maximum temperature of $204 \text{ }^\circ\text{C}$ under an applied bias of 4 V . However, as can be seen from Figure 3.6 (c), Ag NW thin film began to lose its stability around 17^{th} minute, then the temperature gradually decreased between 17^{th} and 20^{th} minutes. On the contrary, when the applied bias is increased incrementally, Ag NW network better adapts itself to the temperature rise and higher temperatures can be obtained. This is clearly shown in Figure 3.8. TTFH sample with a nanowire density of $1.6 \text{ NW}/\mu\text{m}^2$, a temperature of $225 \text{ }^\circ\text{C}$ has been attained under an applied potential of 4.5 V , while the same sample was failing once a temperature of $204 \text{ }^\circ\text{C}$ was attained under 4 V . This adaptation is tentatively attributed to the incremental increase in the thermal expansion of NWs in the case of incremental increase in the applied bias, rather than

an immediate thermal expansion in the case of immediate application of bias. Therefore, contacts between nanowires stay intact and resist failure. Thus, higher applied biases can be reached and higher temperatures can be attained.

3.4. Effect of Repetitive Heating and Cooling Cycles

Performance of TTFHs with a density of $1.6 \text{ NW}/\mu\text{m}^2$ under repetitive heating and cooling cycles for an applied bias of 3 V is provided in Figure 3.9.

For these measurements, voltage was applied for 10 minutes and then it was turned off for another 10 minutes. This cycle was repeated for 5 times.

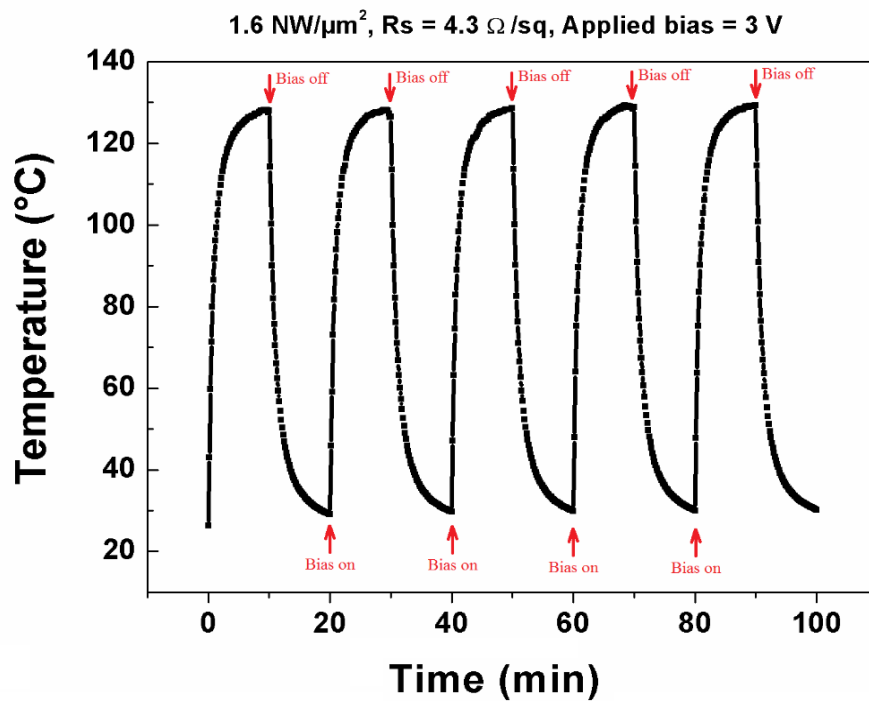


Figure 3.9. Change in temperature as a function of time under repetitive heating (3 V) and cooling cycles for a TTFH with a NW density of $1.6 \text{ NW}/\mu\text{m}^2$.

It is observed that the thermal performance of the TTFH with a NW density of 1.6 $\text{NW}/\mu\text{m}^2$ is not affected by repetitive heating (3 V) and cooling cycles at least for the 5 cycles investigated herein. Thermal response is almost identical in each loop, indicating that structure of Ag NW networks remain intact. This stability is particularly important if TTFHs are going to be used for a commercial application.

In the case of the application of a higher voltage (11 V) that of which Ag NW thin film (with NW density of 0.5 $\text{NW}/\mu\text{m}^2$) can barely withstand, network structure begins to deteriorate after two heating and cooling cycles. This behavior is shown in Figure 3.10.

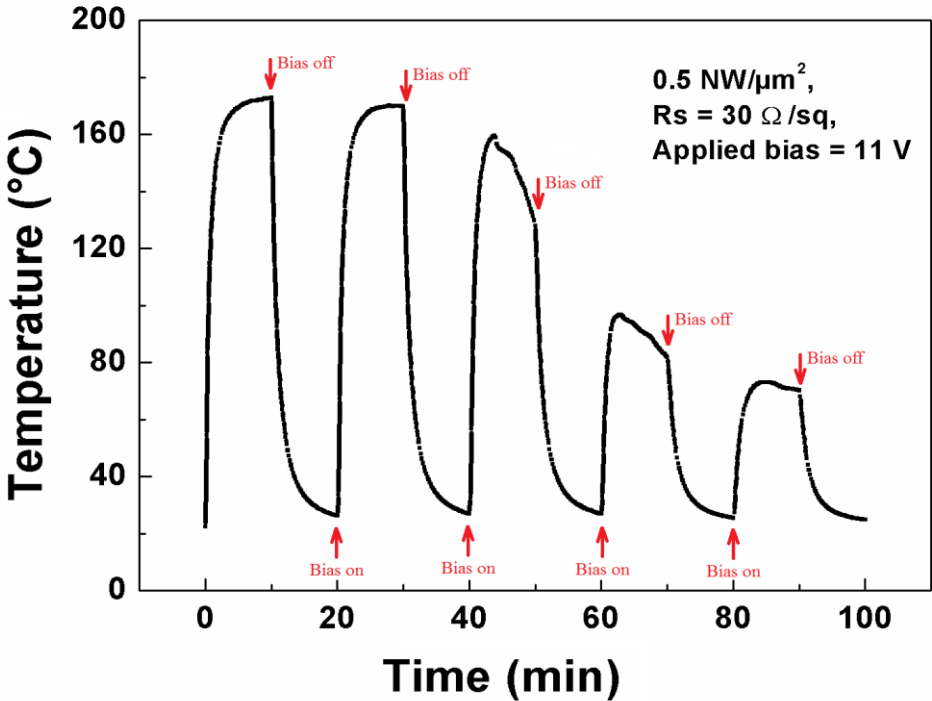


Figure 3.10. Change in temperature as a function of time under repetitive heating (11 V) and cooling cycles for a TTFH with a NW density of 0.5 $\text{NW}/\mu\text{m}^2$.

3.5. Long Term Stability of TTFHs

The change in temperature as a function of time under a fixed (3 V) long term bias for a TTFH with a NW density of $1.6 \text{ NW}/\mu\text{m}^2$ is provided in Figure 3.11. For these measurements a constant bias of 3 V was applied for 22 hours. While measuring the sample temperature, one of the thermocouples were detached from the sample surface to monitor the ambient temperature. Results of this measurement are also provided within the same figure.

In the first 10 seconds of the experiment the temperature increased to $118 \text{ }^\circ\text{C}$ under the applied bias of 3 V. In the following 20 minutes the temperature increased gradually to $126 \text{ }^\circ\text{C}$. This $8 \text{ }^\circ\text{C}$ temperature increase is attributed to annealing of the Ag NWs due to Joule heating, because this particular sample had not been annealed after spray coating step in the fabrication process. Therefore, PVP residues at NW junctions were slowly removed due to Joule heating. This resulted in the temperature to rise up to $126 \text{ }^\circ\text{C}$ until most of the PVP is removed.

After the first 20 minutes, it was observed that the temperature increased 4 % (from $126.6 \text{ }^\circ\text{C}$ to $131.8 \text{ }^\circ\text{C}$) during the 22 hours period. This increase is attributed to removal of the final PVP residues and possible strengthening of the Ag NW junctions in the long term. The Ag NW networks were found to be stable under long term biasing.

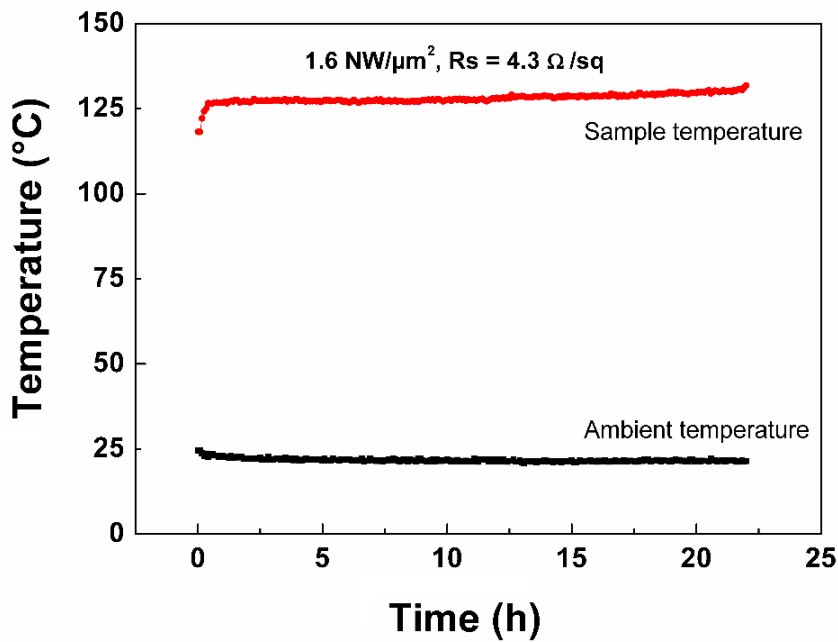


Figure 3.11. Change in temperature as a function of time for a TTFH with a NW density of $1.6 \text{ NW}/\mu\text{m}^2$ which is long term biased at 3V.

3.6. Reproducibility of the TTFH Characteristics

TTFH characteristics were checked after 50 days to investigate the reproducibility of the devices. First of all, it was found that the sheet resistance of a TTFH with a nanowire density of $1.6 \text{ NW}/\mu\text{m}^2$ increased to $4.9 \text{ } \Omega/\text{sq}$ from its initial value of $4.3 \text{ } \Omega/\text{sq}$ after 50 days. It is worth mentioning that the sample was stored in ambient conditions within this period. Change in the temperature response for this TTFH is given in Figure 3.12. Measurement results right after the fabrication of TTFH devices and after 50 days of storage are plotted.

Change in the sheet resistance and therefore the thermal response was attributed to the possible oxidation of Ag NWs under ambient conditions. Oxidation results in an

increase of sheet resistance of the sample, lowering the temperature attained under an applied bias. Nevertheless, a 14% increase in the sheet resistance coupled with a 12.5% decrease in the maximum attainable temperature obtained after 50 days can be declared as satisfactory. The performance of the Ag NW thin films even after 50 days still nearly meets the minimum standards required by industry for TCEs, $T \geq 90\%$ and $R_s < 100 \Omega/\text{sq}$ as set by Hewlett-Packard (see ref [22] of Scardaci et al. 2011¹¹).

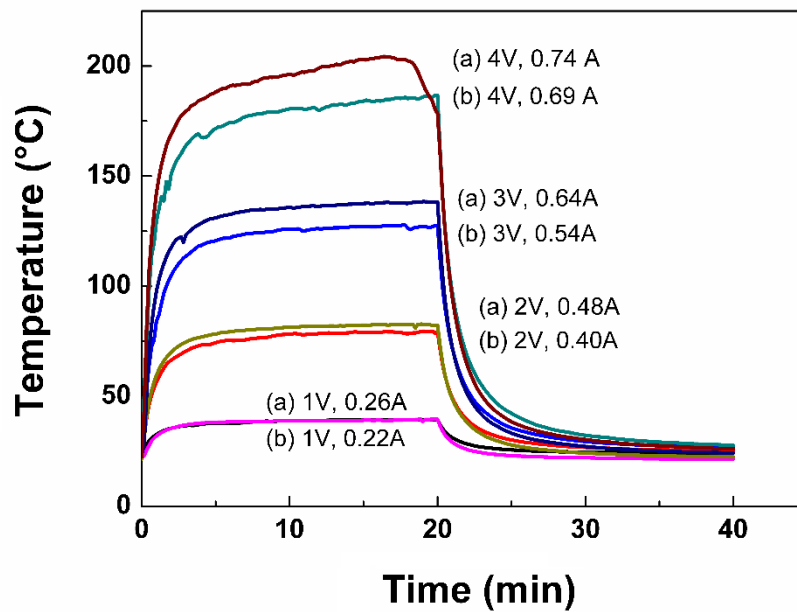


Figure 3.12. Change in temperature as a function of time for a TTFH with a NW density of $1.6 \text{ NW}/\mu\text{m}^2$. Results for (a) right after the fabrication of TTFH devices ($R_s = 4.3 \Omega/\text{sq}$), and (b) after 50 days of storage ($R_s = 4.9 \Omega/\text{sq}$), are plotted.

3.7. Flexibility

Effect of bending on thermal response characteristics of Ag NW networks coated on PET substrates (4 cm x 5 cm) under an applied bias of 4 V is given in Figure 3.13. It is observed that concave configuration under an applied bias of 4 V results in higher attained temperatures (up to 90 °C) than those attained in straight (up to 80 °C) and convex (up to 72 °C) configurations. Higher attained temperatures during concave bending can be attributed to an increase in the number of physical contact points between NWs due to an increased NW spatial density. On the other hand, convex bending results in a decrease in NW spatial density which in turn decreases the number of physical contact points.

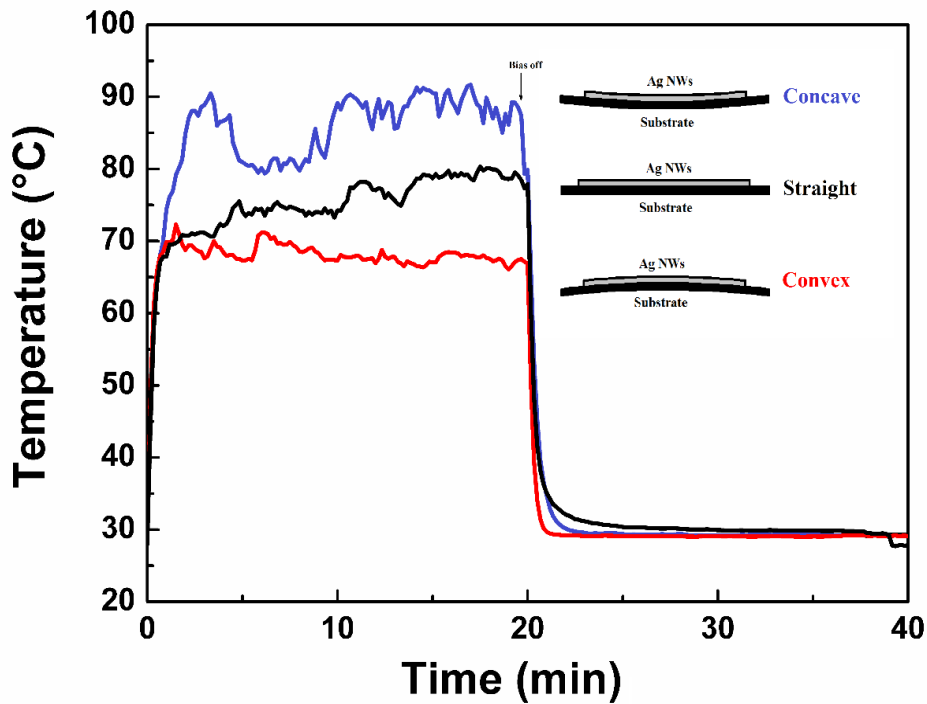


Figure 3.13. Thermal response characteristics of Ag NW networks coated on flexible PET substrates in straight and bended (concave and convex) configurations under an applied bias of 4 V.

CHAPTER 4

CONCLUSIONS AND FUTURE WORK

4.1. Summary of the Work

There is increased interest in transparent heaters for defogging and deicing applications. Ag NW networks are appealing candidates due to their high thermal performance coupled with high optical transmittance. On the other hand, conventional transparent thin film heater materials, such as ITO, have increasing prices worldwide due to indium's scarcity.

In this study, Ag NW networks were reproducibly deposited on different substrates. TTFHs were fabricated through the deposition of Ag contacts in appropriate geometry determined in this thesis. Effect of NW density, applied voltage and bending on the thermal output of the TTFHs were investigated. Failure mechanism of the TTFHs was also investigated in conjunction to the optoelectronic characteristics of thin films.

Firstly, the effect of parallel contact geometry, 4-contact geometry and opposite corners 2-contact geometry on the thermal characteristics of TTFHs were studied. It was found that sharp corners having small distances in between, result in high electrical flux and must be avoided. Therefore, TTFHs with two parallel contacts on the opposite sides are crucial for the most homogeneous temperature distribution, withstand higher temperatures and currents before the failure of Ag NW networks.

Secondly, the effect of NW density was studied. It was found that the density of NWs can simply be increased through increasing the number of spray coating cycles. Number of NW contacts increase with NW density, which in turn increases the conductivity and reduces the sheet resistance. On the other hand, since there are more NWs per unit area in a denser sample, transparency is decreased due to higher absorption (or higher scattering) of light passing through the TTFH.

Next, the effect of bias voltage on the thermal behaviour of TTFHs with various NW densities was investigated. It was found that the achieved maximum temperature was 204 °C under an applied potential of 4 V for the sample with a Ag NW density of 1.6 NW/ μm^2 . However, this maximum temperature was not stable. The maximum stable temperature was 180 °C under an applied bias of 9 V for the sample with a Ag NW density of 0.6 NW/ μm^2 . In addition to that, the sample with a Ag NW density of 0.5 NW/ μm^2 reached a maximum temperature of 175 °C under an applied bias of 11 V. All Ag NW network samples' %T and R_s nearly meet the minimum standards required by industry for TCEs, $T \geq 90\%$ and $R_s < 100 \Omega/\text{sq}$ in this work.

Next, failure mechanism of Ag NWs was investigated. As the temperature was increased, Ag NWs began to melt and Ag began to accumulate at nanowire junctions. Melting of thin Ag NWs resulted in Ag NWs getting even thinner. As the temperature continued to increase, Ag NWs began to fail and rupture. This resulted in a decrease in the number of current pathways, which began to increase the sheet resistance of the networks upto kilohms and then to megaohms. Finally, NWs broke into discontinuous segments, where TTFHs failed and thermal response dropped to zero.

The effect of repetitive heating and cooling cycles on the performance of TTFHs was studied. Thermal response was found to be almost identical in each cycle, indicating that the structure of Ag NW networks remain intact.

It was also found that the Ag NW networks were stable under 22 hours long term biasing.

Lastly, the effect of bending on the thermal response characteristics of Ag NW networks deposited onto PET substrates was studied. It was found that attained temperatures were higher in concave configuration compared to those attained in straight and convex configurations.

4.2. Future Work

Spray deposited Ag NW networks can easily be scratched. This adhesion problem is not only important because it decreases TTFH performance, but also it might bring health concerns due to potential hazards of scratched Ag NWs. Thus a protective coating on Ag NWs is highly desirable. Another possibility is to embed Ag NWs into a polymeric substrate.

Oxidation/sulphidization mechanism of Ag NWs and the resulting reduction in thermal performance of Ag NW based TTFHs may as well be investigated. Prevention of oxidation/sulphidization again through the use of a protective coating on Ag NWs or through embedding of Ag NWs into a polymeric substrate can also be investigated.

REFERENCES

- (1) Janas, D.; Koziol, K. K. *Carbon* **2013**, *59*, 457–463.
- (2) Li, J.; Liang, J.; Jian, X.; Hu, W.; Li, J.; Pei, Q. *Macromol. Mater. Eng.* **2014**, *299*, 1403–1409.
- (3) Tian, H.; Xie, D.; Yang, Y.; Ren, T.-L.; Lin, Y.-X.; Chen, Y.; Wang, Y.-F.; Zhou, C.-J.; Peng, P.-G.; Wang, L.-G.; Liu, L.-T. *Applied Physics Letters*, **2011**, *Vol. 99, No. 25*, 253507.
- (4) Celle, C.; Mayousse, C.; Moreau, E.; Basti, H.; Carella, A.; Simonato, J.-P. *Nano Research* **2012**, *Vol. 5 No. 6*, 427-433.
- (5) Gordon R.G. *MRS Bulletin* **2000**, 52-57.
- (6) Honeywell Sensing and Control Application Note, www.honeywell.com/sensing (accessed July 20, 2015).
- (7) Volman, V.; Zhu, Y.; Raji, A.-O.; Genorio, B.; Lu, W.; Xiang, C.; Kittrell, C.; Tour, J. M. *ACS Appl. Mater. Interfaces* **2014**, *6*, 298–304.
- (8) Liu, C. -H.; Yu, X. *Nanoscale Research Letters* **2011**, *6*, 75.
- (9) Minco, “Flexible Heaters Design Guide”, HDG01(A).
- (10) Minco, Thermofoil™ Heaters, Bulletin HS-202(B).
- (11) Scardaci V.; Coull R.; Lyons P.E.; Rickard D.; Coleman J.N. *Small* **2011**, *7*, *No. 18*, 2621–2628.
- (12) Facchetti, A.; Marks, T. J. “Transparent Electronics: From Synthesis to Applications”, **2010**, John Wiley & Sons Ltd, Chapter 2 “Transparent Oxide Semiconductors: Fundamentals and Recent Progress”, H. Hosono.
- (13) Sorel, S.; Bellet, D.; Coleman, J.N.; *ACS Nano* **2014**, *vol. 8, no 5*, 4805–4814.
- (14) Yakuphanoglu, F.; Anand, R.S. *Syn. Met.* **2010**, *vol. 160, no. 21*, 2250–2254.,
- (15) AEI August 2014, Dempa Publications, Inc., Tech Focus, “Best-in-Class Touchscreens with Silver Nanowires”.

- (16) http://www.eizoglobal.com/library/basics/basic_understanding_of_touch_panel/ (accessed July 20, 2015).
- (17) Kiruthika, S.; Gupta, R.; Kulkarni, G. U. *RSC Adv.* **2014**, *4*, 49745–49751.
- (18) Kwon, N.; Kim, K.; Heo, J.; Yi, I.; Chung, I. *Nanotechnology* **2014**, *25*, 265702.
- (19) Kim, T. Y.; Kim, Y. W.; Lee, H. S.; Kim, H.; Yang, W. S.; Suh, K. S. *Adv. Funct. Mater.* **2013**, *23*, 1250–1255.
- (20) Gupta, R.; Rao, K. D. M.; Srivastava, K.; Kumar, A.; Kiruthika, S.; Kulkarni, G.U. *Appl. Mater. Interfaces* **2014**, *6*, 13688–13696.
- (21) Wang, S.; Zhang, X.; Zhao, W. *Journal of Nanomaterials* **2013**, *2013*, 456098.
- (22) Zhang, X., Yan, X., Chen, J., Zhao, J. *Carbon* **2014**, *69*, 437–443.
- (23) Kim, D., Zhu L., Jeong, D. -J., Chun, K., Bang, Y. -Y., Kim, S. -R., Kim, J. -H., Oh, S. -K. *Carbon* **2013**, *63*, 530–536.
- (24) Cheong, H.-G.; Song, D.-W.; Park, J.-W. *Microelectron. Eng.* **2015**, *146*, 11–18.
- (25) Ji, S.; He, W.; Wang, K.; Ran, Y.; Ye, C.; *Small* **2014**.
- (26) Hsu, P.-C.; Liu, X.; Liu, C.; Xie, X.; Lee, H.R.; Welch, A.J.; Zhao, T.; Cui, Y. *Nano Lett.* **2015**, *15*, 365–371.
- (27) Rao, K. D. M.; Kulkarni, G. U. *Nanoscale* **2014**, *6*, 5645–5651.
- (28) Janas, D.; Koziol, K. K. *JOACE* **2014**, *2*, 150.
- (29) Jang, H.-S.; Jeon, S. K.; Nahm, S. H. *Carbon* **2011**, *49*, 111–116.
- (30) Jung, D.; Kim, D.; Lee, K. H.; Overzet, L. J.; Lee, G. S. *Sensors and Actuators A* **2013**, *199*, 176–180.
- (31) Kang, T. J.; Kim, T.; Seo, S. M.; Park, Y.J.; Kim, Y. H. *Carbon* **2011**, *49*, 1087–1093.

- (32) Kim, D.; Lee, H. -C.; Woo, J. Y.; Han, C. -S. *J. Phys. Chem. C* **2010**, *114*, 5817–5821.
- (33) Kim, D.; Lee, H. -C.; Woo, J. Y.; Han, C.-S. *Proceedings of 10th IEEE International Conference on Nanotechnology, Joint Symposium with Nano Korea* **2010**.
- (34) Wu, Z. P.; Wang, J.N. *Physica E* **2009**, *42*, 77–81.
- (35) Yoon, Y.-H.; Song, J.-W.; Kim, D.; Kim, J.; Park, J.-K.; Oh, S.-K.; Han C.-S.; *Adv. Mater.* **2007**, *19*, 4284–4287.
- (36) Bae, J. J.; Lim, S. C.; Han, G. H.; Jo, Y. W.; Doung, D. L.; Kim, E. S.; Chae, S. J.; Huy, T. Q.; Luan, N. V.; Lee, Y. H. *Adv. Funct. Mater.* **2012**, *22*, 4819–4826.
- (37) Kang, J.; Kim, H.; Kim, K.S.; Lee, S.-K.; Bae, S.; Ahn, J.-H.; Kim, Y.-J.; Choi, J.-B.; Hong, B.H. *Nano Lett.* **2011**, *11*, 5154–5158.
- (38) Lee, B.-J.; Jeong, G.-H. *Current Applied Physics* **2012**, *12*, 113–117.
- (39) Wang, J.; Fang, Z.; Zhub, H.; Gao, B.; Garner, S.; Cimo, P.; Barcikowski, Z.; Mignerey, A.; Hub, L. *Thin Solid Films* **2014**, *556*, 13–17.
- (40) Im, K.; Cho, K.; Kim, J.; Kim, S. *Thin Solid Films* **2010**, *518*, 3960–3963.
- (41) Yang, K.; Cho, K.; Im, K.; Kim, S. *Materials Research Bulletin* **2015**, *63*, 194–198.
- (42) Ahn, B.D.; Oh, S.H.; Hong, D.U.; Shin, D.H.; Moujoud, A.; Kim, H. J. *Journal of Crystal Growth* **2008**, *310*, 3303–3307.
- (43) Kim, J. H.; Ahn, B. D.; Kim, C. H.; Jeon, K. A.; Kang, H. S.; Lee, S. Y. *Thin Solid Films* **2008**, *516*, 1330–1333.
- (44) Li J.; Liang J.; X. Jian; W. Hu; J. Li; Qibing Pei *Macromol. Mater. Eng.* **2014**, *299*, 1403–1409.
- (45) Calnan, S.; Tiwari, A.N. *Thin Solid Films* **2010**, *518*, 1839–1849.
- (46) Chopra, K.L., Major, S., Pandya, D.K. *Thin Solid Films* **1983**, *102*, 1.

- (47) Minami, T.; Miyata, T., *Presentation given at SPIE* **2008**, January 23rd.
- (48) Liu, H.; Avrutin, V.; Izyumskaya, N.; Özgür, Ü.; Morkoç H. *Superlattices and Microstructures* **2010**, *48*, 458–484.
- (49) Wager, J. F.; Keszler, D. A.; Presley, R. E. *Transparent Electronics*, **2008**, Springer.
- (50) <http://www.tibtech.com/conductivity.php> (accessed July 20, 2015).
- (51) Bellingham, J. R.; Phillips, W. A.; Adkins, C. J. *J Mater Sci Lett* **1992**, *11*, 263-265
- (52) Kawazoe, H.; Yasukawa, M.; Hyodo, H.; Kurita, M.; Yanagi, H.; Hosono, H. *Nature* **1997**, *389*, 939-942.
- (53) Rupperecht, G. Z. *Phys.* **1954**, *139*, 504.
- (54) Tuna, O.; Selamat, Y; Aygun, G.; Ozyuzer, L. *J. Phys. D: Appl. Phys.* **2010**, *43*, 055402.
- (55) Khaligh, H. H., Silver Nanowire Transparent Electrodes: Fabrication, Characterization, and Device Integration, (Thesis, M.S.), Electrical and Computer Engineering –Nanotechnology, University of Waterloo, 2013.
- (56) Cairns, D.R.; Witte, R.P.; Sparacin, D.K.; Sachsman, S.M.; Paine, D.C.; Crawford, G.P.; Newton, R.R. *Appl. Phys. Lett.* **2000**, *76*, 1425.
- (57) Sui, D.; Huang, Y.; Huang, L.; Liang, J.; Ma, Y.; Chen, Y. *Small* **2011**, *7*, 3186.
- (58) Wang, X.; Zhi, L.; Muellen, K. *Nano. Lett.* **2008**, *8*, 323.
- (59) Sayers, S. A.; Gagiano, M. A.; Moore, T. D. Patent Cooperation Treaty (PCT) WO 2010/131050 A1
- (60) Sylvain, T. US006341554B2.
- (61) Kawashima, T.; Ezure, T.; Okada, K.; Matsui, H.; Goto, K.; Tanabe, N. *J. Photochem. Photobiol. A* **2004**, *164*, 199–202.
- (62) Bae, J.W.; Lee, S.W.; Yeom, G.Y. *Electrochem. Soc.* **2007**, *154*, D34–D37.

- (63) Elmer, K. *J. Phys., D, Appl. Phys.* **2001**, *34*, 3097.
- (64) Agura, H.; Suzuki, H.; Matsushita, T.; Aoki, T.; Okuda, M. *Thin Solid Films* **2003**, *445*, 263–267.
- (65) Park, S.-M.; Ikegami, T.; Ebihara, K. *Thin Solid Films* **2006**, *513*, 90–94.
- (66) Ohta, H.; Orita, M.; Hirano, M.; Tanji, H.; Kawazoe, H.; Hosono, H. *Appl. Phys. Lett.* **2000**, *76*, 2740–2742.
- (67) Qadri, S. B.; Kim, H.; Khan, H. R.; Pique, A.; Horowitz, J. S.; Chrisey, D.; Kim, W. J.; Skelton, E. F. *Thin Solid Films* **2000**, *377–378*, 750–754.
- (68) Kim, H.; Gilmore, C. M.; Horwitz, J. S.; Pique, A.; Murata, H.; Kushto, G. P.; Schlaf, R.; Kafa, Z. H.; Chrisey, D. B. *Appl. Phys. Lett.* **2000**, *76*, 259–261.
- (69) Iijima, S. *Nature* **1991**, *56*, 354.
- (70) Chen, K.-R.; Yeh, H.-F.; Chen, H.-C.; Liu, T.-J.; Huang, S.-J.; Wu, P.-Y.; Tiu, C. *Advances in Chemical Engineering and Science* **2013**, *3*, 105-111.
- (71) Nirmalraj, P. N.; Lyons, P. E.; De, S.; Coleman, J. N.; Boland, J. *J. Nano Lett.* **2009**, *9*, 3890 .
- (72) <https://en.wikipedia.org/wiki/Graphene> (accessed July 25, 2015).
- (73) Lupu, N. “Nanowires Science and Technology” **2010**, Intech.
- (74) De, S.; Higgins, T.; Lyons, P. E.; Doherty, E. M.; Nirmalraj, P. N.; Blau, W. J.; Boland, J. J.; Coleman, J. N. *ACS Nano* **2009**, *3*, 1767.
- (75) <http://www.digitimes.com/news/a20140415VL200.html> (accessed July 20, 2015).
- (76) Langley, D.; Giusti, G.; Mayousse, C.; Celle, C.; Bellet, D.; Simonato, J.-P. *Nanotechnology* **2013**, *24*, 452001.
- (77) Langley, D. P.; Lagrange, M.; Giusti, G.; Jiménez, C.; Bréchet, Y.; Nguyenb, N. D.; Bellet, D. *Nanoscale* **2014**, *6*, 13535.

- (78) De, S.; Higgins, T. M.; Lyons, P. E.; Doherty, E. M.; Nirmalraj, P. N.; Blau W. J.; Boland, J. J.; Coleman, J. N. *ACS Nano* **2009**, *3*, 1767-1774.
- (79) Kholmanov, I. N.; Stoller, M. D.; Edgeworth, J.; Lee, W. H.; Li, H.; Lee, J.; Barnhart, C.; Potts, J. R.; Piner, R.; Akinwande, D.; Barrick, J. E.; Ruoff, R. S. *ACS Nano* **2012**, *6*, 6, 5157–5163.
- (80) Chen, T. L.; Ghosh, D. S.; Mkhitarian, V.; Pruneri, V. *ACS Appl. Mater. Interfaces* **2013**, *5*, 11756–11761.
- (81) Choi, K. -H.; Kim, J.; Noh, Y. -J.; Na, S. -I.; Kim, H.-K. *Solar Energy Materials & Solar Cells* **2013**, *110*, 147–153.
- (82) Koo, B. -R.; Ahn, H. -J. *Applied Physics Express* **2014**, *7*, 075002.
- (83) Golobostanfard, M. R.; Abdizadeh, H.; Mohammadi, S.; Baghchesara, M. A. *Solar Energy Materials & Solar Cells* **2015**, *132*, 418–424.
- (84) Rathmell, A. R.; Nguyen, M.; Chi, M.; Wiley, B. J. *Nano Lett.* **2012**, *12*, 3193–3199.
- (85) Jeong, C.; Nair P.; Khan, M.; Lundstrom, M.; Alam, M. A. *Nano Lett.* **2011**, *11*, 5020–5025.
- (86) Kumar, A. B. V. K.; Bae, C.; Piao, L.; Kim, S. -H. *Materials Research Bulletin* **2013**, *48*, 2944–2949.
- (87) Haacke, G. *J. Appl. Phys.* **1976**, *47*, 4086.
- (88) Pichitpajongkit, A.; Lee J.; Eom, H.; Yang, D.; Yoon, J.; Lee, J.; Park, I.; “Joule Heating and Thermal Analysis of Silver Nanowire Random Network”.
- (89) Ragab, T.; Basaran, C. *J. Appl. Phys* **2009**, *106*, 063705.
- (90) Rutherglen, C.; Burke, P. J. *Small* **2009**, *5*, 884–906.
- (91) Tsuchiya, K.; Li, Y.; Saka, M. *Nanoscale Research Letters* **2014**, *9*, 239.
- (92) Toimil Molares, M. E.; Balogh, A. G.; Cornelius, T. W.; Neumann R.; Trautmann C. *Appl. Phys. Lett.* **2004**, *85*, 5337.

- (93) Jeong, W.; Kim, K.; Kim, Y.; Lee, W.; Reddy, P. *Scientific Reports* **2014** *4*, 4975.
- (94) Black, J. R. *IEEE Transactions on Electron Devices* **1969**, *4*, 338-347.
- (95) Kim, S. H.; Choi, B. S.; Kang, K.; Choi, Y. S.; Yang, S. I. *J. Alloys Compd.* **2007**, *433*, 261.
- (96) Grijalva, A. S.; Urbina, R. H.; Silva, J. F. R.; Borja, M. A.; Barraza, F. F. C.; Amarillas, A. P. *Physica E* **2005**, *25*, 438.
- (97) Mazur, M. *Electrochem. Commun.* **2004**, *6*, 400.
- (98) Huang, L. M.; Wang, H. T.; Wang, Z. B.; Mitra, A.; Bozhilov, K. N.; Yan, Y. S. *Adv. Mater.* **2002**, *14*, 61.
- (99) Xu, J.; Hu, J.; Peng, C. J.; Liu, H. L.; Hu, Y. J. *Colloid Interface Sci.* **2006**, *298*, 689.
- (100) Wang, Z.; Liu, J.; Chen, X.; Wan, J.; Qian, Y. *Chem.—Eur. J.* **2005**, *11*, 160.
- (101) Zhou, Y.; Yu, S.; Wang, C.; Li, X.; Zhu, Y.; Chen, Z. *Adv. Mater.* **1999**, *11*, 850.
- (102) Zou, K.; Zhang, X. H.; Duan, X. F.; Meng, X. M.; Wu, S. K. *J. Cryst. Growth* **2004**, *273*, 285.
- (103) Braun, E.; Eichen, Y.; Sivan, U.; Yoseph, G. B. *Nature* **1998**, *391*, 775.
- (104) Keren, K.; Krueger, M.; Gilad, R.; Ben-Yoseph, G.; Sivan, U.; Braun, E. *Science* **2002**, *297*, 72.
- (105) Berchmans, S.; Nirmal, R. G.; Prabakaran, G.; Madhu, S.; Yegnaraman, V. J. *Colloid Interface Sci.* **2006**, *303*, 604.
- (106) Kong, L. B.; Lu, M.; Li, M. K.; Li, H. L.; Guo, X. Y. *J. Mater. Sci. Lett.* **2003**, *22*, 701.
- (107) Piquemal, J. Y.; Viau, G.; Beaunier, P.; Verduraz, F. B.; Fievet, F. *Mater. Res. Bull.* **2003**, *38*, 389.

- (108) Gasga, J. R.; Elechiguerra, J. L.; Liu, C.; Bragado, A. C.; Carrizales, J. M. M.; Yacamán, M. J. *J. Cryst. Growth* **2006**, *286*, 162.
- (109) Coskun, S.; Aksoy, B.; Unalan, H.E. *Cryst. Growth Des.* **2011**, *11*, 4963–4969.
- (110) Fievet, F.; Lagier, J. P.; Blin, B.; Beaudoin, B.; Figlarz, M. *Solid State Ionics* **1989**, *Vol. 32, No. 3*, 198-205.
- (111) Fievet, F.; Lagier, J. P.; Figlarz, M. *MRS Bull.* **1989**, *14*, 29.
- (112) Viau, G.; Fievet-Vincent, F.; Fievet, F. *Solid State Ionics* **1996**, *84*, 259.
- (113) Toneguzzo, G.; Viau, O.; Acher, F.; Fievet-Vincent, F.; Fievet, F. *Adv. Mater.* **1998**, *10*, 1032.
- (114) Bonet, F.; Delmas, V.; Grugeon, S.; Urbina, R. H.; Silvert, P. Y.; Tekaiia-Elhsissen, K. *Nanostruct. Mater.* **1999**, *11*, 1277.
- (115) Wiley, B.; Sun, Y. G.; Mayers, B.; Xia, Y. N. *Chemistry-A European Journal* **2005**, *Vol. 11, No. 2*, 454-463.
- (116) Zang, Z.; Zhao, B.; Hu, L. *J. Solid State Chem.* **1996**, *121*, 105.
- (117) Roosen, A. R.; Carter, W. C. *Physica A* **1998**, *232*, 261.
- (118) Liu, C. -H.; Yu, X. *Nanoscale Res. Lett.* **2011**, *6*, 75–82.
- (119) Deegan, R. D.; Bakajin, O.; Dupont, T. F.; Huber, G.; Nagel, S. R.; Witten, T. A. *Nature* **1997**, *389*, 827-829.
- (120) Kim, T.; Canlier, A.; Kim, G. H.; Choi, J.; Park, M.; Han, S. M. *ACS Appl. Mater. Interfaces* **2012**, *5*, 788–794.
- (121) Hauger, T. C.; Al-Rafia, S. M. I.; Buriak, J. M. *ACS Appl. Mater. Interfaces* **2013**, *5*, 12663–12671.
- (122) Kaempgen, M.; Lebert, M.; Haluska, M.; Nicoloso, N.; Roth, S. *Adv. Mater.* **2008**, *20*, 616–620.

- (123) Tenent, R. C.; Barnes, T. M.; Bergeson, J. D.; Ferguson, A. J.; To, B.; Gedvilas, L. M.; Heben, M. J.; Blackburn, J. L. *Adv.Mater.* **2009**, *21*, 3210–3216.
- (124) Park, J. W.; Shin, D. K.; Ahn, J.; Lee, J. Y. *Semicond. Sci. Technol.* **2014**, *29*, 015002.
- (125) Preston, C.; Xu, Y.; Han, X.; Munday, J. N.; Hu, L. *Nano Res.* **2013**, *6*, 461–468.
- (126) Coskun, S.; Ates, E. S.; Unalan, H. E. *Nanotechnology* **2013**, *24*, 125202.
- (127) Coskun, S. Synthesis of Silver Nanowires Through Polyol Process, (Thesis, M.S.), Department of Materials Science and Engineering Middle East Technical University, 2012.